Åbo Akademi University

Björn Törngren

Development and application of plasmonic materials for dye- and polymer-sensitized solar cells

Development and application of plasmonic materials for dye- and polymer-sensitized solar cells

Björn Törngren

Laboratory of Physical Chemistry
Faculty of Science and Engineering
Åbo Akademi University
Åbo, Finland
2018

Supervised by

Academic lecturer Jan-Henrik Smått
Laboratory of Physical Chemistry
Åbo Akademi University
Finland

Co-supervised by

Professor Jouko Peltonen
Laboratory of Physical Chemistry
Åbo Akademi University
Finland

Reviewed by

Professor Paul R. Berger
Department of Electrical and Computer Engineering
The Ohio State University
USA

Associate Professor Gerrit Boschloo
Department of Chemistry – Ångström Laboratory
Uppsala University
Sweden

Opponent

Professor Paul R. Berger
Department of Electrical and Computer Engineering
The Ohio State University
USA

ISBN 978-952-12-3704-1 (Print)
ISBN 978-952-12-3705-8 (Digital)
Painosalama Oy – Turku, Finland 2018

Acknowledgments

The work presented in this thesis was carried out at the Laboratory of Physical Chemistry, Åbo Akademi University. Much of this work has been done in collaboration with the Department of Physics at Åbo Akademi and the RCAST Laboratory at the University of Tokyo. The Academy of Finland, Åbo Akademi University Foundation, Magnus Ehrnrooth Foundation and Fortum Foundation are gratefully acknowledged for their financial support.

This thesis could not have been possible without the immense help and support from my supervisor Jan-Henrik Smått, who was always there to support me and guide me forward. I am also very thankful to Professor Jouko Peltonen for his support and for giving me the opportunity to work at Fyke.

I am very grateful to Professor Ronald Österbacka for his advice and support, and to Professor Hiroshi Segawa and professor Takaya Kubo for their hospitality and for enabling me to go and visit the RCAST Laboratory. The stay in Tokyo was very fruitful, interesting and inspiring.

I wish to thank all my colleagues and co-authors for their valuable input and support. I especially wish to thank my very good friend Dr. Jawad Sarfraz, with whom I have had numerous interesting discussions on both scientific and unscientific matters. I also wish to thank Dr. Simon Sandén for (trying) to help me understand the physics parts of my work and for his assistance and guidance during my visit to Japan. Regarding practical issues, I am very grateful to Christina Luojola and Kenneth Stenlund for keeping us all in check and everything in order in the lab.

Furthermore, I am honored to have had Professor Paul R. Berger from the Ohio State University and Professor Gerrit Boschloo from Uppsala University as the reviewers of this thesis. I really appreciate their valuable input and comments.

Finally, I am deeply thankful for all my friends and family for all their support during the years.

Björn Törngren

Åbo, 2018

Abstract

Among the numerous solar cell technologies, emerging thin film solar cells, such as dye-sensitized solar cells, offer the possibility for large-scale integration using sustainable and low-cost materials. In these thin devices, controlling the light absorption on the nanoscale is of crucial importance in order to bring them to their full potential. Plasmonic particles can be utilized to tailor the optical response due to their unique size and shape dependent properties. However, successful integration of these particles into the device structures require careful control of the surface properties as well as chemical and thermal stability.

In this thesis, plasmonic materials with suitable optical properties were designed, synthesized and integrated into polymer- and dye-sensitized solar cells. The chemical and thermal stability of these particles was studied, and their optical effects were modeled. The particles were mixed into printable titanium dioxide (TiO_2) pastes or suspensions. The pastes or suspensions were deposited as porous films and the impact of these composite films on the photovoltaic performance of the devices was evaluated.

Gold particles with a protective thin silica shell were synthesized using different coating methods. It was discovered that the coating method greatly influences the shell formation and that the shell quality is of crucial importance for the stability of the gold cores in the chemical environment of the devices. Anisotropic plasmonic particles were also utilized. Gold nanorods with different aspect ratios and thus different optical response were synthesized and added to TiO_2 suspensions. However, it was discovered that the nanorods deform at the temperatures normally used for processing the TiO_2 films. A TiO_2 suspension suitable for low-temperature processing was developed, and the TiO_2 films containing nanorods could be prepared with minimal deformation occurring. An enhancement of the current density of the plasmonic devices could be seen, which was correlated to an increase in the incident photon to electron conversion efficiency (IPCE) spectra due to near- and far-field effects originating from the plasmonic particles.

Furthermore, the impact of the composite semiconductor layer thickness on the device performance was studied. Devices with the thinnest semiconductor layer showed the largest enhancement from the plasmonic particles. This result was further confirmed with modelling of the near- and far-field effects of the plasmonic particles, showing a greatly increased absorption close to the particle surface.

These findings indicate the need for careful control in the design of plasmonic nanoparticles, as well as show the great potential for utilizing plasmonic materials in solar cells.

Svensk sammanfattning

Av de många olika solcellsteknologierna som är tillgängliga idag, har de s.k. tredje generationens solceller, såsom Grätzel-celler, egenskaper som är omöjliga att uppnå med konventionella solceller. Dessa nya solcellsteknologier gör det möjligt att utnyttja hållbara och billiga material samt integrera cellerna i stor skala i byggnader samt på flexibla ytor. För att utnyttja potentialen av dessa tunna solceller till fullo, är kontrollen av ljusabsorptionen på nanometerskala en kritisk faktor. På grund av sina unika optiska egenskaper kan plasmoniska partiklar utnyttjas för att skräddarsy den optiska responsen i solcellerna. Dessa optiska egenskaper påverkas av både partiklarnas form samt storlek. För att integrera dessa partiklar i solcellerna krävs det en noggrann kontroll över partiklarnas ytegenskaper samt en god kemisk och termisk stabilitet hos partiklarna.

I avhandlingen utvecklades framställdes plasmoniska partiklar som optimerades för integration i Grätzel-celler känsliggjorda med färgämnen och polymerer. Partiklarnas kemiska och termiska stabilitet studerades samt deras optiska effekter modellerades. Partiklarna blandades med i titandioxid (TiO_2)-pastan eller -suspensioner, som deponerades och sintrades till porösa filmer. Dessa kompositfilmers inverkan på solcellernas optiska samt fotovoltaiska egenskaper utvärderades.

Guldnanopartiklar med ett skyddande tunt kiseldioxidskal syntetiserades med olika beläggningsmetoder. Beläggningsmetoden hade en stor inverkan på skalets formation samt att skalets kvalitet är kritisk för guldkärnans stabilitet i den kemiska omgivningen i solcellerna. Även anisotropiska stavformade guldpartiklars inverkan på solcellerna undersöktes. Stavformade guldnanopartiklar med olika aspektration, och således olika optiska egenskaper, framställdes samt tillsattes till TiO_2-suspensioner. Dessa stavformade partiklar deformerade dock vid de höga temperaturerna som normalt används vid framställning av porösa TiO_2 filmer. För att åtgärda detta, utvecklades TiO_2-supensioner lämpliga för processering vid lägre temperaturer än konventionella metoder. Komposit guld/TiO_2 filmer gjorda med denna metod uppvisade minimal deformation av de stavformade partiklarna. En ökning av den ljusinducerade strömmen i solcellerna innehållande plasmoniska partiklar kunde observeras. Denna ökning korrelerades till en förbättring vid högre våglängder på grund av förstärkningar i det elektromagnetiska fältet nära de plasmoniska partiklarna.

Även inverkan av guld/TiO_2 filmens tjocklek på solcellernas prestanda undersöktes. Celler med det tunnaste halvledarlagret uppvisade den största förstärkningen från de plasmoniska partiklarna. Modellering av de plasmoniska partiklarnas närfältseffekter visade en skarp förstärkning i ljusabsorptionen nära partiklarnas yta. Denna förstärkning kan i sin tur ge upphov till en förstärkning av ljusabsorptionen hos färgämnesmolekyler som befinner sig nära partiklarna.

Upptäckterna i denna avhandling visar behovet av en noggrann kontroll över framställningen av plasmoniska nanopartiklar samt de visar även potentialen av att utnyttja plasmoniska material i solceller.

List of included publications

Paper I: **B. Törngren**, K. Akitsu, A. Ylinen, S. Sandén, H. Jiang, J. Ruokolainen, M. Komatsu, T. Hamamura, J. Nakazaki, T. Kubo, H. Segawa, R. Österbacka and J.-H. Smått, *Investigation of plasmonic gold-silica core-shell nanoparticle stability in dye-sensitized solar cell applications*, Journal of Colloid and Interface Science, 427, 54–61 (2014)
DOI: 10.1016/j.jcis.2013.11.085

Paper II: **B. Törngren**, S. Sandén, J.O. Nyman, A. Tiihonen, H. Jiang, J. Ruokolainen, J. Halme, R. Österbacka and J.-H. Smått, *Minimizing structural deformation of gold nanorods in plasmon-enhanced dye-sensitized solar cells*, Journal of Nanoparticle Research, 19, 365 (2017)
DOI: 10.1007/s11051-017-4062-9

Paper III: S. Sandén, K. Akitsu, **B. Törngren**, A. Ylinen, J.-H. Smått, T. Kubo, M. Matsumura, N. Otani, H. Segawa and R. Österbacka, *Plasmon-Enhanced Polymer-Sensitized Solar Cells*, The Journal of Physical Chemistry C, 119, 5570–5576 (2015)
DOI: 10.1021/jp5097458

Contributions of the author

Paper I: The author was responsible for the core-shell nanoparticle synthesis, the TiO_2 paste preparation, the device preparation, the material and device measurement and characterization, the analysis of the results and writing the first draft. T. Hamamura and M. Komatsu deposited the TiO_2 films, prepared the DSSC devices and carried out the solar cell measurements. A. Ylinen and S. Sandén performed the particle and device modeling. H. Jiang performed the TEM measurements.

Paper II: The author was responsible for the core-shell nanoparticle synthesis, the TiO_2 paste preparation, the device preparation, the material and device measurement and characterization, the analysis of results and writing the first draft. A. Tiihonen performed the device preparations and the device measurements together with the author. H. Jiang performed the TEM measurements with in situ heating and J.O. Nyman performed the SWLI measurements.

Paper III: The author was responsible for the core-shell nanoparticle synthesis, the material characterization, the analysis of the results and writing part of the first draft. S. Sandén and K. Akitsu performed the device preparation and the solar cell measurements. A. Ylinen and S. Sandén performed the particle modelling. M. Matsumura and N. Otani performed the polymer synthesis.

Supporting publications

SI: P. Ihalainen, H. Majumdar, T. Viitala, **B. Törngren**, T. Närjeoja, A. Määttänen, J. Sarfraz, H. Härmä, M. Yliperttula, R. Österbacka and J. Peltonen, *Application of Paper-Supported Printed Gold Electrodes for Impedimetric Immunosensor Development*, Biosensors, 3, 1–17 (2013)
DOI: 10.3390/bios3010001

SII: J. Massera, M. Vassallo-Breillot, **B. Törngren**, B. Glorieux and L. Hupa, *Effect of CeO_2 doping on thermal, optical, structural and in vitro properties of a phosphate based bioactive glass*, Journal of Non-Crystalline Solids, 402, 28–35 (2014)
DOI: 10.1016/j.jnoncrysol.2014.05.006

SIII: J. Massera, B. Sevrette, L. Petit, J. Koponen, **B. Törngren**, B. Glorieux, L. Hupa and M. Hupa, *Effect of partial crystallization on the thermal, optical, structural and Er^{3+} luminescence properties of silicate glasses*, Materials Chemistry and Physics, 147, 1099–1109 (2014)
DOI: 10.1016/j.matchemphys.2014.06.064

SIV: J. Sarfraz, A. Määttänen, **B. Törngren**, M. Pesonen, J. Peltonen and P. Ihalainen, *Sub-ppm electrical detection of hydrogen sulfide gas at room temperature based on printed copper acetate–gold nanoparticle composite films*, RSC Advances, 5, 13525–13529 (2015)
DOI: 10.1039/C4RA17256F

SV: A. Määttänen, P. Ihalainen, **B. Törngren**, E. Rosqvist, M. Pesonen and J. Peltonen, *Hierarchically structured self-supported latex films for flexible and semi-transparent electronics*, Applied Surface Science, 364, 37–44 (2016)
DOI: 10.1016/j.apsusc.2015.12.088

SVI: O. Sandberg, M. Nyman, S. Dahlström, S. Sandén, **B. Törngren**, J.-H. Smått and R. Österbacka, *On the validity of MIS-CELIV for mobility determination in organic thin-film devices*, Applied Physics Letters, 110, 153504 (2017)
DOI: 10.1063/1.4980101

SVII: J. Sarfraz, M. Borzenkov, E. Niemelä, C. Weinberger, **B. Törngren**, E. Rosqvist, M. Collini, P. Pallavicini, J. Eriksson, J. Peltonen, P. Ihalainen and G. Chirico, *Photo-thermal and cytotoxic properties of inkjet-printed copper sulfide films on biocompatible latex coated substrates*, Applied Surface Science, 435, 1087–1095 (2018)
DOI: 10.1016/j.apsusc.2017.11.203

List of abbreviations

3D	Three-dimensional
AFM	Atomic force microscopy
APTMS	(3-Aminopropyl)trimethoxysilane
a-Si:H	Hydrogenated amorphous silicon
AuNP	Gold nanoparticle
AuNR	Gold nanorod
$Au@SiO_2$ NP	Gold-silica core-shell nanoparticle
$Au@SiO_2$ NR	Gold-silica core-shell nanorod
CIGS	Copper indium gallium selenide
CTAB	Cetyltrimethylammonium bromide
c-Si	Crystalline silicon
CZTS	Copper zinc tin sulfide
DSSC	Dye-sensitized solar cell
FTO	Fluorine-doped tin oxide
HOMO	Highest occupied molecular orbital
IPCE	Incident photon conversion efficiency
ITO	Indium-doped oxide
I-V	Current-voltage
LUMO	Lowest unoccupied molecular orbital
LSPR	Localized surface plasmon resonance
mc-Si	Multi-crystalline silicon
MJ	Multi-junction
MPTMS	(3-Mercaptopropyl)trimethoxysilane
MSC	Mesoscopic solar cell
NIR	Near-infrared
OPV	Organic photovoltaic(s)
P3HT	Poly(3-hexylthiophene-2,5-diyl)
PEDOT	Poly(3,4-ethylenedioxythiophene)
PSSC	Polymer-sensitized solar cell
PV	Photovoltaic(s)
PVP	Poly(vinylpyrrolidone)
QD	Quantum dot
QDPV	Quantum dot photovoltaics
sc-Si	Single-crystalline silicon
SEM	Scanning electron microscopy
SWLI	Scanning white light interferometry
TCO	Transparent conductive oxide
TEM	Transmission electron microscopy
UV-vis	Ultraviolet-visible
XRD	X-ray diffraction

Contents

1 Introduction and outline

Solar photovoltaics (PV) is one of the very few low carbon emission energy technologies with the potential for large scale applications. The utilization of solar PV has grown rapidly in recent years along with great improvements in technology, price, and performance of PV systems. These improvements have resulted in a dramatic decrease in the median price of residential PV installations: from 12.4 $/W in 1998 to 4.3 $/W in 2014.[1] However, these prices are greatly affected by governmental policies and subsidies and are thus subject to fluctuations.

In order to remain competitive with fossil fuel technologies and to enable the adaptation of thin film solar technologies, which usually suffer from lower efficiencies and thus higher costs, further advances are needed for continued increase of PV utilization at acceptable costs. There are three general challenges for PV: reducing the cost of installed capacity, improving the availability of technologies, and enabling large scale production at low cost. The first two challenges are mainly socio-economic issues, whereas the latter challenge can potentially be solved by research and development of new materials and processing methods.

After decades of development, the leading solar PV technology today is wafer-based crystalline silicon (c-Si) solar cells.[2] It is technologically mature and enables manufacturing of modules at large scale. However, the production of these solar cells is both energy- and material-intensive and the physical properties of silicon limit the production of thinner devices. A number of emerging thin film technologies that are at the research stage today, e.g. copper zinc tin sulfide (CZTS) solar cells, dye-sensitized solar cells (DSSCs) and perovskite solar cells, use Earth-abundant materials and can be made thinner as well as deposited on flexible substrates. These properties give them the potential to provide superior performance with lower manufacturing complexity and cost in the future.[3]

When decreasing the thickness and material use of PV devices, light management on the nanoscale becomes crucial (i.e. controlling which parts of the light spectrum are absorbed/scattered and how photons move in the material). This is a complex issue and numerous approaches exist for the light management in thin film devices.[4] One approach is the utilization of plasmonic materials, where the optical response can be tuned by varying the size and shape of the material.[5]

In this thesis, the design of plasmonic materials was investigated and their effect on the optical properties, as well as their impact on the performance of DSSCs and polymer-sensitized solar cells (PSSCs), was studied. When incorporating plasmonic materials into these devices, several crucial factors need to be considered. The plasmonic materials need to be designed with suitable optical properties matching that of the active material in the device. The materials need to withstand the processing conditions and the environment in the cells without deformation or dissolution nor should they affect the structure of the semiconductor layer.

Furthermore, the materials should have minimal undesirable effects on the device performance, i.e. not affect the charge mobility or quenching the charge carriers.

In Paper I, gold-silica core-shell nanoparticles were synthesized and incorporated into the titanium dioxide (TiO_2) photoanode in DSSCs. Four different methods for preparing thin silica coatings on the gold nanoparticles were studied, giving coatings with a thickness of 1–20 nm in thickness. The chemical stability of the core-shell nanoparticles towards the commonly used liquid iodide/triiodide electrolyte in DSSCs was investigated. The PV properties of the DSSC devices were studied, and an enhancing effect could be observed for the devices with incorporated plasmonic particles.

In Paper II, anisotropic gold-silica core-shell nanorods with different aspect ratios were synthesized and incorporated into the TiO_2 photoanode in DSSCs. Thermal stability tests indicated that the nanorods started to deform at temperatures over 200 °C. A composite gold nanorod/TiO_2 paste suitable for low-temperature processing was developed and the structure of the deposited mesoporous TiO_2 layer was evaluated. The PV properties of the DSSC devices prepared by this low-temperature processing method were studied.

In Paper III, a new type of polymer sensitizer was used as a light absorber instead of the commonly used ruthenium-based dyes utilized in the previous studies. The plasmonic effect of the particles was modeled and the interaction with the polymer sensitizer was investigated. Spherical gold-silica core-shell nanoparticles were synthesized and incorporated in the TiO_2 semiconductor layer. The thickness of the semiconductor layer was varied between 1–5 μm and the effect on the device performance was studied.

2 Background and literature review

The Sun delivers constantly around 174000 TW to the upper level of Earth's atmosphere, at an average power density of 1366 W/m^2, known as the solar constant.[6] This value is reduced to around 1000 W/m^2 perpendicular to the Earth's surface due to atmospheric absorption and scattering, and further reduced locally due to geographical and seasonal variations. Figure 1 shows the incoming solar radiation spectrum perpendicular to the Earth's surface. The spectrum demonstrates that the highest intensity of the incoming radiation is in the visible wavelengths, i.e. between 500 to 750 nm.

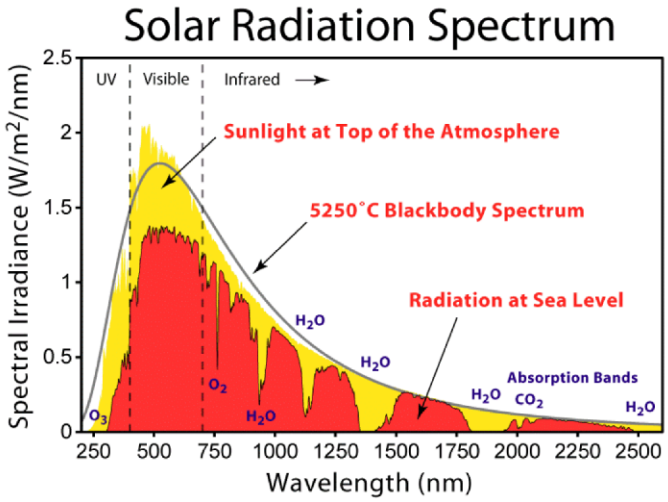

Figure 1. Solar radiation spectrum perpendicular to the Earth's surface.[7]

Despite the variations in the power density, solar energy is one of the most equally distributed energy resources in the world. No location in the world lacks direct local access to sunlight. The same cannot be said for fossil fuels and other extractive energy resources. The main challenge to utilize solar energy is not its availability but rather the technical/economical aspects.

The most widely used solar energy technology is solar photovoltaics (PV). Driven by light, solar cells operate at ambient temperatures without any moving parts. They are also very scalable, a small array is (in theory) not less efficient per unit area than a large one, unlike other technologies such as wind turbines or generators which lose efficiency with decreased scale.[8]

However, the current PV technologies can only utilize a small part of the solar spectrum. Therefore, there is a need for strategies to increase the light absorption (especially at higher wavelengths), as well as to increase the efficiency and to reduce the production costs.

2.1 Photovoltaic effect

In very general terms, the conversion of sunlight (photons) to electricity (electrons) by solar cells can be divided into the following steps:[3]

1. A solar photon is absorbed by the active part of the system.
2. The active part of the system contains occupied (valence band) and unoccupied (conduction band) states separated by an energy gap (bandgap).
3. Upon absorption of a photon with sufficient energy to overcome the bandgap, light induced transition of electrons can occur from the valence band to the conducting band.
4. Selective extraction of charge carriers (electrons/holes) to contacts occurs.

These steps are used to describe the PV process in all working devices, with some modifications for organic/excitonic solar cells where the electrons and holes are initially coupled as excitons (electron/hole pairs).[3]

The active material in solar cells is usually a narrow bandgap semiconductor, which absorbs light in the ultraviolet-visible (UV-vis) range.[3,4] The bandgap is the minimum amount of energy required for an electron to break free from its bound state in the valence band and move to the conduction band. When this energy requirement is met (i.e. a photon with high enough energy is absorbed by the semiconductor), the electron is excited and can move to the conduction band and participate in the conduction. A hole is created in the valence band where the electron was previously located, and this hole also participates in the conduction.

A major factor in optimizing the PV conversion process is matching the absorption of the active layer of the device with the incoming sunlight spectrum. The absorption properties of the active material determine the dimensions and the geometry of the device. The device has to be thick enough to absorb the light efficiently, but it should also be thin enough to ensure the electron/hole extraction without recombination. The electrons/holes should be extracted at separate contacts, meaning that the contacts should be selective for one carrier and prevent the extraction of the other.[9]

2.2 Solar cell technologies

There are numerous types of solar cell technologies available, which can be classified in various ways such as material use and complexity, charge separation, etc.[3,9] A commonly used method is to classify them according to the semiconducting material used: wafers or thin films. The thin films can be further classified according to the technological maturity as commercial or emerging thin films. This classification is illustrated in Figure 2, where the most common wafer and thin film technologies are shown.[10] It is worth noting that a device using newer technologies or materials does not necessarily mean a better all-round device, since the older technologies are also constantly improving and have currently a much greater

market penetration. The newer generations can be rather seen as complementary approaches to expand the utilization of solar energy, for instance by enabling the integration of solar cells into building facades or onto vehicle surfaces.[11]

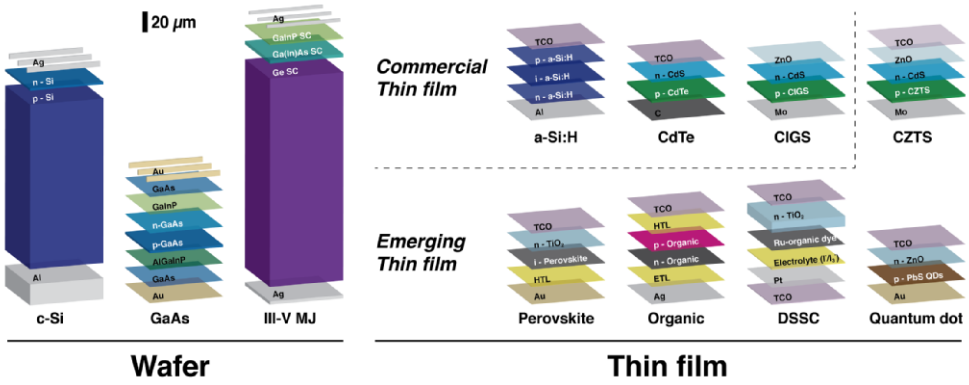

Figure 2. Typical PV device structures, divided into wafer-based and thin film technologies. Primary absorber layers are labeled with white text, and layer thicknesses are shown to scale.[10]

2.2.1 Wafer-based materials and solar cell devices

Crystalline silicon (c-Si) is one of the oldest and most widespread materials used in solar cells, representing about 90% of the commercial modules sold today.[8,12] Silicon is one of the most abundant elements on Earth and widely used in the semiconductor industry. Silicon solar cells are classified either as single-crystalline (sc-Si) or multi-crystalline (mc-Si), depending on the manufacturing process. Single crystals are typically grown using the Czochralski process, where a small silicon crystal is dipped into molten silicon and slowly withdrawn at a constant rate.[13] This results in a cylindrical single crystal ingot, which can be cut into wafers and further processed. Multi-crystalline wafers are formed by block casting liquid silicon, forming a silicon slab, which can then be cut into wafers. This approach results in wafers with randomly oriented crystalline grains with sizes of around 1 cm^2.[14] The production of mc-Si is cheaper than sc-Si, however the crystalline grains will reduce their cell performance compared with sc-Si cells.[15]

In general, c-Si solar cells provide high efficiency at a relatively low cost and long device lifetimes. One fundamental limitation of c-Si is its indirect bandgap, which results in weak light absorption and thus requires wafers with thicknesses of around 200–300 μm. This limits the device thinness and flexibility, thus impacting the possibility for module integration.[16] Other drawbacks are the material purity requirements and the energy intensive processing needed for manufacturing.[17]

Gallium arsenide (GaAs) is a compound semiconductor with strong absorption, a direct bandgap, and very low non-radiative energy loss. Due to its direct bandgap,

a thin film of the material is enough to ensure sufficient light absorption.[18] Thin and flexible GaAs films are manufactured using epitaxial lift-off of crystalline films grown on rigid substrates.[19] GaAs-based devices hold the world record for the highest-efficiency single-junction solar cell at 28.8%.[20] However, GaAs solar cells have not yet been produced in higher volumes due to the more expensive materials and manufacturing costs compared to other wafer-based technologies.

III-V multi-junction (MJ) solar cells use stacks of several single-junction cells with different semiconductor materials. By using semiconducting materials with different bandgaps and thus different light absorbing properties, MJ solar cells can absorb light efficiently across a wide range of the solar spectrum. Elements from group III (Al, Ga, In) and group V (N, P, As, Sb) are used to form high-quality semiconducting crystalline films with variable bandgaps.[21] MJ solar cells have the highest efficiencies of all solar cell technologies, above 30% at one sun illumination and up to 46% under concentrated sunlight.[22] Unfortunately, due to the complex structure and the manufacturing process, MJ cells are currently far too expensive for traditional terrestrial applications. They are however used extensively in space applications, due to their high power-to-weight ratio, high radiation resistance and low temperature sensitivity. Future challenges for III-V MJ technologies include improving the processing for large areas, reducing the use of materials, and optimizing the cell architectures.[23]

2.2.2 Commercial thin film solar cell devices

Following the rigid wafer-based devices, the next technological development is based on devices using thin semiconducting materials deposited on a support carrier such as glass, metal or plastic. The devices utilize abundant and low-cost materials suitable for large-scale printing and deposition methods, which enables low-cost manufacturing processes.[11]

Hydrogenated amorphous silicon (a-Si:H) is a non-crystalline form of silicon, which exhibits a stronger absorption than c-Si, although with a larger bandgap and thus reduced absorption range.[24] Due to its strong absorption, the devices can be made thinner and more flexible than c-Si cells. MJ cells can be made by combining a-Si:H cell with nanocrystalline silicon or amorphous silicon-germanium alloys without lattice-matching requirements.[25] The a-Si:H cells are cheap and relatively easy to produce, making them suitable for small-scale and low-power applications. However, the light-induced degradation of the PV performance of the cells (the Staebler-Wronski effect) and their low efficiency compared with other technologies limit their widespread use.[25,26]

Cadmium telluride (CdTe) is a good semiconductor for solar energy harvesting, due to its direct bandgap and strong light absorption across the solar spectrum.[27] CdTe solar cells have the highest efficiencies (~20%) and shortest energy payback time compared to other thin film technologies.[28] High-throughput processing can be

used to manufacture the cells, which combined with the high efficiency leads to the lowest module cost of current commercial thin film PV technologies. However, the toxicity of cadmium and scarcity of tellurium have motivated research for alternative materials that can utilize similar processing methods.[29]

Copper indium gallium diselenide ($CuIn_xGa_{(1-x)}Se_2$, CIGS) is a I-III-VI_2 compound semiconductor with a direct bandgap between 1.0–1.7 eV and a high absorption coefficient. The bandgap can be adjusted by tuning the stoichiometry of the compound, from pure copper indium selenide to pure copper gallium selenide.[30] Utilizing similar methods as CdTe films, CIGS films can be deposited by a variety of solution- and vapor-based techniques onto rigid or flexible substrates, making them suitable for integrated PV applications.[9] Furthermore, CIGS solar cells exhibit high radiation resistance, making their use also feasible in space applications. Challenges in the utilization include variations in film stoichiometry and film integrity as well as the material defects from the processing. Furthermore, the scarcity of elemental indium could limit the large-scale production of CIGS solar cells.[29]

2.2.3 Emerging thin film solar cell devices

Although the utilization of commercial thin film devices is increasing, they are limited in their applications. Emerging thin film technologies have the potential to be made transparent or in a variety of colors, which enables their integration into different products. Examples of the different technologies are shown in Figure 3.

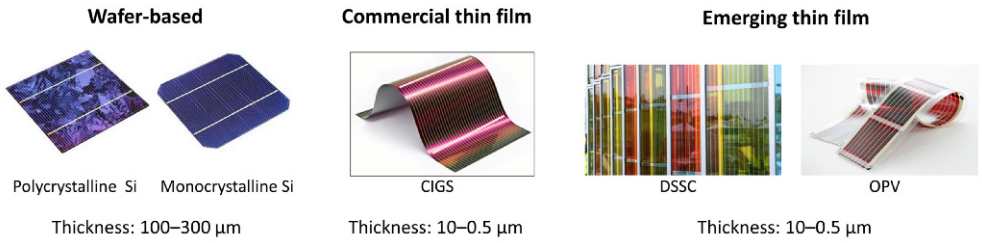

Figure 3. Examples of devices of different solar cell technologies with active layer thicknesses.[31,32]

Copper zinc tin sulfide (Cu_2ZnSnS_4, CZTS) is an alternative to CIGS, utilizing cheap and abundant materials, which can be processed with similar techniques.[33] CZTS has similar properties as CIGS with regards to bandgap and absorption coefficient, but lower carrier lifetimes due to defects and grain boundaries. As with CIGS films, the material defects as well as the variations in material stoichiometry and film integrity remain a challenge.[34] One key challenge involves minimizing secondary phases with sulfur-rich compounds (i.e. CuS, ZnS, SnS) in the material. These secondary phases are hard to detect but have a detrimental effect on the solar cell performance.

Organic photovoltaics (OPV) use semiconducting organic polymers or organic small molecules instead of inorganic semiconductor materials to absorb incident light. These organic materials consist mostly of abundant elements, which can be tailored for desired functionalities.[35] The materials can be solution processed and assembled into thin films by low-cost deposition methods, such as inkjet printing and thermal evaporation. Similarly to other thin film solar cells, they can also be applied onto a variety of substrate materials.[36] The organic materials are usually large conjugated π-systems, i.e. systems where carbon atoms covalently bond with alternating single and double bonds. By changing the length and the functional group of the polymers, the bandgap can be tuned.[37] Due to the wide range of materials that can be used, and the possibility for solution processing, OPVs have the potential to be used for a several applications. They are applicable for powering autonomous sensors due to their light weight, and they can potentially be produced as disposable and/or semi-transparent materials.[38] The main challenges for OPVs are the inefficient transport of excitons and charge carriers, low efficiencies and poor long-term stability.

Colloidal quantum dot photovoltaics (QDPV) use semiconducting inorganic nanocrystals, also known as quantum dots (QDs), to absorb light. In contrast to bulk materials, where the bandgap is determined by the choice of material, the bandgap of QDs can be tuned by simply changing the size of the crystal.[39] The QDs can be grown in a range of sizes, thus making it possible to obtain a range of different bandgaps without modifying any other components or processing methods. This allows the harvesting of near-infrared (NIR) photons, which is difficult to obtain with other PV technologies, as well as the possibility to produce MJ cells using a single material system.[40] The possibility to use wet-chemistry approaches for synthesis and deposition of QDs makes them easy to fabricate without expensive equipment, although currently they are mostly produced in smaller batches. Current challenges include low efficiencies due to the low charge carrier mobility and open-circuit voltages, and an incomplete understanding of the QD surface chemistry.[41]

Dye-sensitized solar cell (DSSC) technology is among the most mature and well understood emerging thin film PV technologies.[42] The DSSC consists of a nanoporous inorganic scaffold (typically a TiO_2 film) which is sensitized with a light-absorbing organic dye (usually ruthenium complexes). The main differences from the other technologies are the separation of light absorption and electron transport into two different components (organic dye/inorganic film), and the use of a liquid electrolyte to transport ions to the counter electrode and regenerate the dye.[43]

DSSCs have achieved efficiencies of up to 12.3% and may benefit from low-cost materials, simple assembly, and the possibility of flexible modules. Key challenges involve limited long-term stability under illumination and high temperatures, low absorption in the NIR, and low open-circuit voltages caused by interfacial recombination.[44] The components and operating principle of DSSCs, since being the

type of solar cells being developed in this thesis, will be discussed in more detail in Section 2.3.

Perovskite solar cells have originated from a modification of solid-state dye-sensitized cells and have very quickly evolved into a separate PV technology. Today, perovskite solar cells are seen as one of the most promising emerging thin film PV technologies. The development has been very rapid, with efficiencies increasing from 10.9% to 22.1% in less than three years.[45] The term perovskite refers to light-absorbing materials with the same crystal structure as calcium titanium oxide ($CaTiO_3$) perovskite mineral. The most commonly used material is a hybrid organic-inorganic lead or tin halide, such as methylammonium lead trihalide ($CH_3NH_3PbX_3$, where X is a halogen atom Cl, Br, I, or a combination thereof).[46] Similarly to CIGS and CZTS films, crystalline perovskite films can be formed at low temperatures by a variety of solution or vapor deposition methods. The perovskite films exhibit high absorption coefficients, long charge carrier diffusion lengths and tunable bandgaps based on the halide content, making them suitable for thin, lightweight and flexible devices. Challenges include the control of film morphology and material properties, high sensitivity to moisture, unproven cell stability, and the use of harmful lead compounds in the materials.[47,48]

An overview of the photon conversion spectra for different solar cell technologies compared with the incoming solar flux is given in Figure 4. The figure demonstrates that many of the emerging thin film technologies are limited in their spectral response, especially in the NIR range at 900 nm and higher, in comparison to the conventional technologies. Thus, it is crucial to understand and control the optical response to fully utilize these novel materials.

2.3 Dye-sensitized solar cells

DSSCs (and some perovskite solar cells) belong to the class of thin film devices referred to as mesoscopic solar cells (MSCs). These cells use three-dimensional (3D) interpenetrating network junctions for the light harvesting, with structural elements in the 2–50 nm range.[49] Due to their porous structure, they have a very large total internal surface area in comparison to their projected area. The semiconductor materials used are usually wide bandgap materials such as TiO_2 or SnO_2. A light-active material can then be adsorbed onto the high internal surface area or be deposited into the porous structure, which results in very high visible light absorption while retaining a low device thickness. Organic light-absorbing dyes or polymers can be adsorbed on the surface of the material (in the case of DSSCs), or hybrid inorganic perovskite materials or QDs can be deposited into the pores (perovskite solar cells, QD cells).[50] Other advantages of the MSCs are that they are inexpensive, scalable and can be solution-processed. They can potentially be produced at costs less than 1 $/W, which is competitive with current energy prices. Some MSC technologies can avoid the expensive and energy-intensive high-vacuum

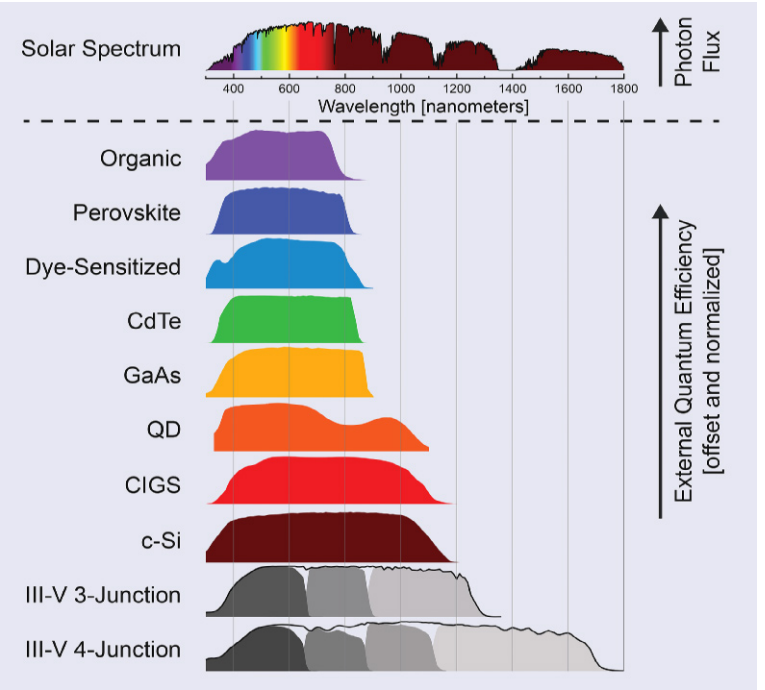

Figure 4. Solar Photon Flux at the Earth's surface and normalized photon conversion spectra for different types of solar cells.[8]

processing and material purification steps needed for other types of thin film solar cells.[51] The materials used in MSCs are usually abundant and of low toxicity, in contrast to the materials used in CdTe and CIGS solar cells (see Section 2.2.2). In this thesis, mainly DSSCs have been investigated.

The development of DSSCs originated in 1971, when zinc oxide electrodes were sensitized with chlorophyll dyes.[52,53] The efficiencies of these devices were low, so it was not until 1991, when Michael Grätzel and Brian O'Regan published their pioneering work using TiO_2 electrodes sensitized with ruthenium dyes with efficiencies over 7%, that the research activities regarding DSSCs greatly increased.[54] The device efficiencies improved steadily, until reaching 11.9% in 2012.[55] The majority of the current research related to DSSCs focuses on improving the stability and increasing the lifetime of the devices, and improving the device integration for commercial applications.[56]

Due to the separation of the solar cell function into different layers of the device, the components can be individually tailored for the desired purpose. DSSCs also perform better under diffuse and ambient light conditions compared to other technologies.[57] This is due to the 3D structure of the photoanode, which scatters light efficiently, making it much less sensitive to the angle of incidence of the incoming light. These properties give the possibility to design solar cells with large

flexibility in the terms of color, shape and transparency. This enables them to be integrated into different products and buildings, which was shown in Figure 3.

However, a drawback of the current embodiment of DSSCs is that their efficiency is still lower than that of sc-Si and mc-Si as well as CdTe and CIGS cells due to the limitations in the material and the physical properties.[49] Many of the components used are very sensitive to water and oxygen and hence the DSSCs need to be carefully sealed to avoid rapid degradation.[44] Although the major breakthrough for DSSCs came already in 1991, so far there has not been any larger commercial utilization of these devices. The three main factors limit the application of DSSCs are low scalability, low stability and low efficiency.

Although one benefit of thin film devices is their scalability, it is limited by some factors in the DSSCs. The iodide electrolyte commonly used in DSSCs is chemically very aggressive and will readily corrode metals in contact with it. This limits the use of (metal) contacts and requires the use of more expensive transparent conductive oxide (TCO) substrates such as fluorine-doped tin oxide (FTO) as well as proper sealing and encapsulation.[44,58] Consequently, the device requires both high extrinsic stability (sealant stability) and high intrinsic stability (dye degradation, electrolyte leakage).

2.3.1 Components in a dye-sensitized solar cell

The general structure of a DSSC is illustrated in Figure 5. The main active component is the light active dye-sensitized photoanode, which is a nanocrystalline mesoporous semiconductor layer deposited on a conductive substrate.[44,59]

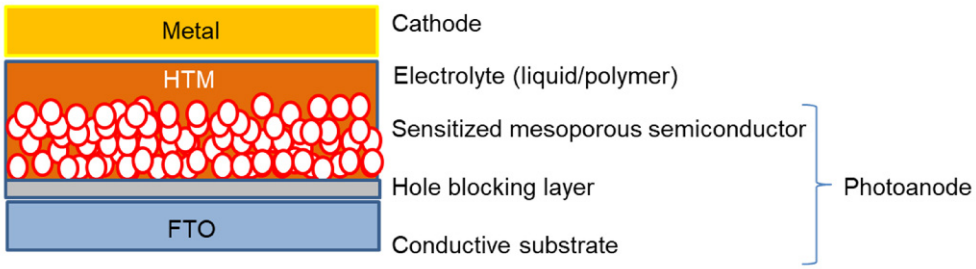

Figure 5. General structural schematic for DSSCs.

2.3.1.1 Photoanode

As was previously mentioned, nanostructured semiconductor films with high surface areas form the core of the DSSCs. The nanostructured films are deposited on a conductive substrate, forming the photoanode component of the DSSC. The substrates used are usually TCO films: FTO glass and indium-doped tin oxide (ITO) glass are commonly used. Flexible substrates such as ITO-coated polyethylene terephthalate films or metal sheets have also been be used as substrates.[60] The

photoanode serves a dual purpose: it forms the support for the sensitizer and acts as a transport medium for electrons from the sensitizer to the external circuit. A large surface area is needed to ensure a high dye loading, and a fast charge transport rate is needed for the efficient electron extraction. The semiconductor material usually consists of nanoparticles of an n-type metal oxide (TiO_2 is commonly used, but ZnO or SnO_2 are also alternatives), formed into about 10 μm nanostructured thick films with a surface area of around 50 m^2/g.[44] This mesoporous structure allows for a 1000-fold larger surface area than its projected area. However, this disordered network consists of numerous grain boundaries, which restrict efficient charge transport and lead to recombination of photo-excited electrons, thus limiting the efficiency of the devices. This has induced the development of numerous approaches trying to enhance the performance of DSSCs:

- The photoanodes can be prepared with different approaches such as sol-gel deposition, spray pyrolysis, atomic layer deposition, etc. This gives a wide range of possibilities to form hierarchical architectures and other structures with controlled porosity, thus controlling the optical properties and electron transport properties of the photoanode.[61]
- Ion doping can be used to adjust the conduction or valance band of the semiconductor and to reduce the recombination and to prolong the electron lifetime in the photoanode.[62]
- Surface modification of the photoanode with insulators (such as SiO_2 or Al_2O_3) or other semiconductors (such as SnO_2 or ZnO_2) can reduce the charge recombination. Also, the incorporation of other materials into the structure, especially graphene or carbon nanotubes can improve the charge transport properties.[63]
- Up/down converting materials (for instance Er^{3+}/Yb^{3+}-doped nanoparticles) can be incorporated into the structure, converting NIR or ultraviolet light into visible light. This will broaden the light harvesting of the device and thus lead to higher current densities.[64]
- Plasmonic materials (e.g. Au, Ag) can be used to enhance the light absorption of the photoanode by localizing incident light and increasing the optical path length due to plasmonic effects. By tuning the size and shape of the plasmonic particles, different optical responses can be achieved, allowing tailoring the response to desired wavelengths.[65] This approach has been the focus of this thesis and will be explained in more detail in Section 2.4.3.

2.3.1.2 Sensitizer

The sensitizer is the light active component of the DSSC, harvesting photons and injecting electrons into the semiconductor material. The sensitizer should have chemical groups that can attach to the semiconductor surface, as well as suitable highest occupied molecular orbital (HOMO) and lowest unoccupied molecular orbital (LUMO) levels for efficient charge injection into the semiconductor and regeneration from the electrolyte. Furthermore, high molar extinction coefficients

in the visible and NIR regions are desirable as well as good photostability and solubility. Dyes based on ruthenium complexes are usually used in DSSCs due to their broad light absorption range and suitable energy levels.[66] However, due to the high cost of ruthenium, other alternatives such as organic or porphyrin dyes are actively investigated.[67] The organic donor-π-acceptor porphyrin dyes and π-conjugated polymers do not contain any expensive elements and show large absorption coefficients. Additionally, polymers can form thicker layers due to the folding of the polymer chain and thus increase the optical density of the photoanode. The polymer thickness is limited by the short exciton diffusion length encountered in these materials, which is typically in the 5–10 nm range. This, however, is much thicker than the monolayer of the dye molecules in standard DSSCs, meaning that the overall thickness of the photoanode can be reduced when using polymer sensitizers. It is worth noting that inorganic materials such as QDs and perovskites were originally used as sensitizers in DSSCs,[66] although they have now evolved into their own technologies, as was discussed in Section 2.2.3. The sensitizers used for the studies in this thesis consisted of the ruthenium dye N719 and a partially hydrolyzed copolymer PT-C 85. Further details of the sensitizers used are given in Section 4.3.

2.3.1.3 Electrolyte

An electrolyte is infiltrated into the sensitized photoanode to function as the medium to selectively transport ions to the counter electrode and to regenerate the oxidized dye. The solubility and ionic mobility coupled with the fast electron transfer kinetics are the crucial factors for the electrolyte. There are three main types of electrolytes (which impact both the efficiency and stability of DSSCs):[68]

- Liquid electrolytes consist usually of the iodide/triiodide redox couple with good kinetic properties, good infiltration and relatively high stability. However, the redox couple is chemically very aggressive and can corrode noble metal particles and contacts. Alternative redox couples consisting of cobalt or copper complexes are also used. The use of liquid electrolytes requires proper sealing, which can be a problem for long-term durability.
- In order to avoid the problems regarding volatility and leakage for liquid electrolytes, quasi-solid-state electrolytes with ionic liquids or polymer gels consisting of redox couples have been investigated. However, they have proven to be thermodynamically unstable and still require proper sealing due to solvent leakage under higher temperatures under solar illumination (up to 80 °C).[69]
- Solid-state electrolytes can also function as hole transporting materials. The materials which have been investigated include inorganic p-type materials (CuI/CuSCN) or organic polymers used in organic PV (poly(3,4-ethylenedioxythiophene)/poly(3-hexylthiophene-2,5-diyl) (PEDOT/P3HT)). However, the filling of the porous structure is an issue when using solid-state electrolytes.[70]

2.3.1.4 Counter electrode

The counter electrode in DSSCs collects the electrons from the external circuit and catalyzes the reduction of the redox electrolyte. High conductivity, good electrocatalytic ability and stability are the main requirements.[71] Noble metals (Pt, Au and Ag) are commonly used due to their high electrolcatalytic activity for the redox couple; however, the corrosion of these materials by the electrolyte is a problem. Carbon materials such as graphene or carbon nanotubes can also be used as inexpensive alternatives due to their high conductivity and corrosion resistance. Inorganic compounds consisting of various sulfides, carbides and phosphides have also been studied, although they still suffer from poor performance and stability. Conductive polymers such as PEDOT have also been investigated as counter electrode materials, especially for flexible DSSCs.[72]

2.3.2 Operating principle

As was mentioned previously in Section 2.3, the functional steps of DSSCs are separated in the different layers of the device. This is in contrast with conventional wafer-based technologies, where the photon to electron conversion and charge transport all take place in the bulk of the semiconductor. The operational principle of a DSSC can be separated into six different steps as illustrated in Figure 6:

1. The dye absorbs a photon and enters an excited state. The lifetime of this excited state is in the range of nanoseconds.
2. The dye injects an electron into the conduction band of the TiO_2. The injection rate is in the femtosecond range, whereas the back reaction (i.e. reduction of the oxidized dye molecule by electrons from the conduction band) is in the μs–ms range. This large difference is the reason for the efficient charge separation in the device.
3. The electron is transported via diffusion through the TiO_2 layer to the electrode. The thickness of the TiO_2 layer determines the maximum diffusion length.
4. The electron diffuses to the anode (TCO) and flows through the external electric circuit.
5. The electron is transferred to the hole-conductive medium at the counter electrode. The most common hole-conductive medium for DSSCs is the iodide/triiodide (I^-/I_3^-) redox couple. The iodine reduction must be orders of magnitude faster than the recombination at the TiO_2/electrolyte interface. The reduction is catalyzed by Pt or other materials.[74]
6. The oxidized dye is regenerated by the redox couple.

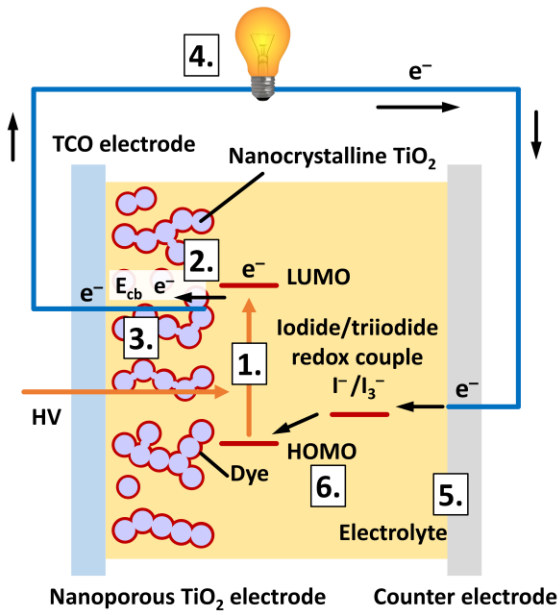

Figure 6. Schematic of the main processes in DSSCs under illumination.[73]

2.4 Plasmonic materials

As was mentioned in Section 2.3.1, there are numerous approaches to enhance the optical path length in thin film materials. Using plasmonic materials has been proven to be an effective method to significantly enhance the light harvesting performance and they have been utilized in a variety of applications,[75-77] including surface-enhanced Raman scattering[78] and biosensing.[79,80]

Light incident on a nanostructured metal surface will give rise to coherent oscillations of the conduction electrons excited by the electromagnetic radiation at the metal-dielectric interface. This effect results in the so-called localized surface plasmon resonance (LSPR) at a specific wavelength, depending on the type of material and the size/shape of the structure. By adjusting the geometry, dimension, and composition of the metal nanostructures, their LSPR can be tailored to capture desired wavelengths of the incoming light. Thus, by utilizing subwavelength plasmonic nanostructures, which complements the absorption by the sensitizer, the total light trapped within the material can be increased and the optical absorption can be improved.[81-83] This improved absorption should also lead to the improved carrier generation and thus result in a better overall power conversion efficiency of solar cell devices. In Figure 7 the solar irradiance spectrum is shown with the absorbance of a selection of plasmonic nanoparticles. From the spectra it is evident that by tuning the size, shape and composition of the plasmonic materials, light absorption in a broad spectral range can be obtained.

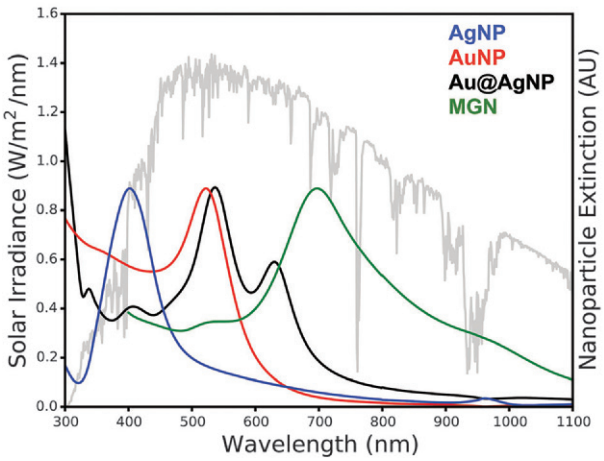

Figure 7. Solar irradiance spectrum and absorption spectra of different plasmonic nanoparticles.[81] AgNP: silver nanoparticles, AuNP: gold nanoparticles, Au@AgNP: core-shell gold-silver nanoparticles, and MGN: multi-branched gold networks.

The benefit of using plasmonic materials for various optical applications is their high extinction cross-sections versus physical cross sections, as illustrated in Figure 8. Due to the plasmonic effect the light enhancement extends beyond the physical dimension of the material. For other optical species (i.e. chromophores or QDs), the light absorption depends on the physical properties and dimensions of the material and thus cannot extend beyond the physical cross-section. Furthermore, the optical properties of the plasmonic metal nanoparticles can be tuned more freely than for other optical species.[84]

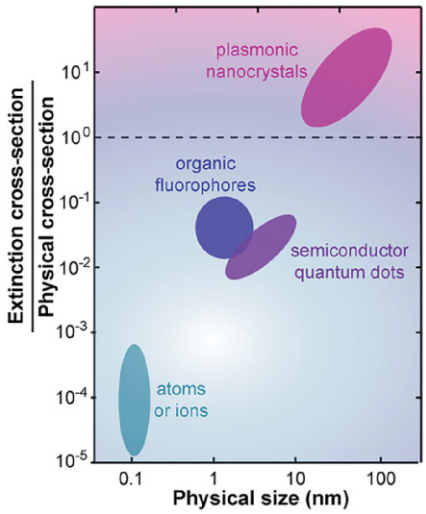

Figure 8. Comparison of extinction and physical cross-section of different optical species.[84]

2.4.1 The plasmonic effect

The term *plasmon* corresponds to a quantum of plasma oscillation. A plasma is a gas where the electric charges can move freely under the influence of electromagnetic or gravitational forces. Comparatively in metallic materials, electrons in the ground state can freely move through the crystal structure. When an electromagnetic wave hits the metal surface, the electron cloud will start oscillating at the surface. This oscillation will be confined close to the metal surface due to the screening properties of the metal. Thus, when the geometrical conditions are filled, this oscillation will result in an evanescent wave propagating along the surface. This wave is called a surface plasmon. However, when the surface plasmon oscillation is confined to the surface of a particle comparable or smaller than the wavelength of light; as in the case of metal nanoparticles, a phenomenon called LSPR will occur.[85] The LSPR gives rise to two main effects; the electric field close to the particle surface is greatly enhanced and the optical absorption has a maximum at the resonance frequency As a note, for textual clarity the term plasmon/plasmonic will be used to refer to localized surface plasmons in this thesis unless otherwise mentioned.

Light incident on a metal nanoparticle gives rise to an oscillation of free electrons in the material since the generated electric field from the light pushes the electrons in the particle to one side. The negative charges accumulate on one side and positive charges accumulate on the other side. These charges attract one another, so if the negative charges are released they will oscillate back and forth with a certain frequency. If the frequency of the incident light matches this natural resonance frequency, large oscillations are produced for all of the free electrons in the metal.

Plasmonic effects can occur in many different materials with adequate charge carrier densities. In noble metals, the plasmonic effects are very prominent due to their high density of conduction band electrons in the material. The more electrons or charge carriers involved in the oscillation, the greater the electrostatic restoring force and thus the resonance frequency. Silver and gold has extensively been used in the study of plasmonic effects due to their high quality plasmonic resonances in the visible range. Silver has the strongest plasmon resonance due to the low energy loss of the material. However, gold is more chemically and physically stable, so it is often used instead. Other materials can also exhibit plasmonic resonances, such as aluminum and highly doped semiconductors, metal chalcogenides and metal oxides, but for visible and NIR resonances, noble metals are commonly used.[86] Furthermore, the LSPR wavelength, extinction cross-section, and local electric field enhancement are all highly dependent on the size, shape, and crystalline structure of the nanocrystal, as well as its surrounding environment.[85,87]

LSPR in plasmonic materials result in various optical and electronic effects, occurring during the excitation and subsequent decay of the created plasmon. These effects can be divided into two main categories: *radiative* and *non-radiative* effects. The radiative and non-radiative effects can manifest with different mechanisms,

resulting in four possible mechanisms for plasmonic enhancement, as shown in Figure 9.

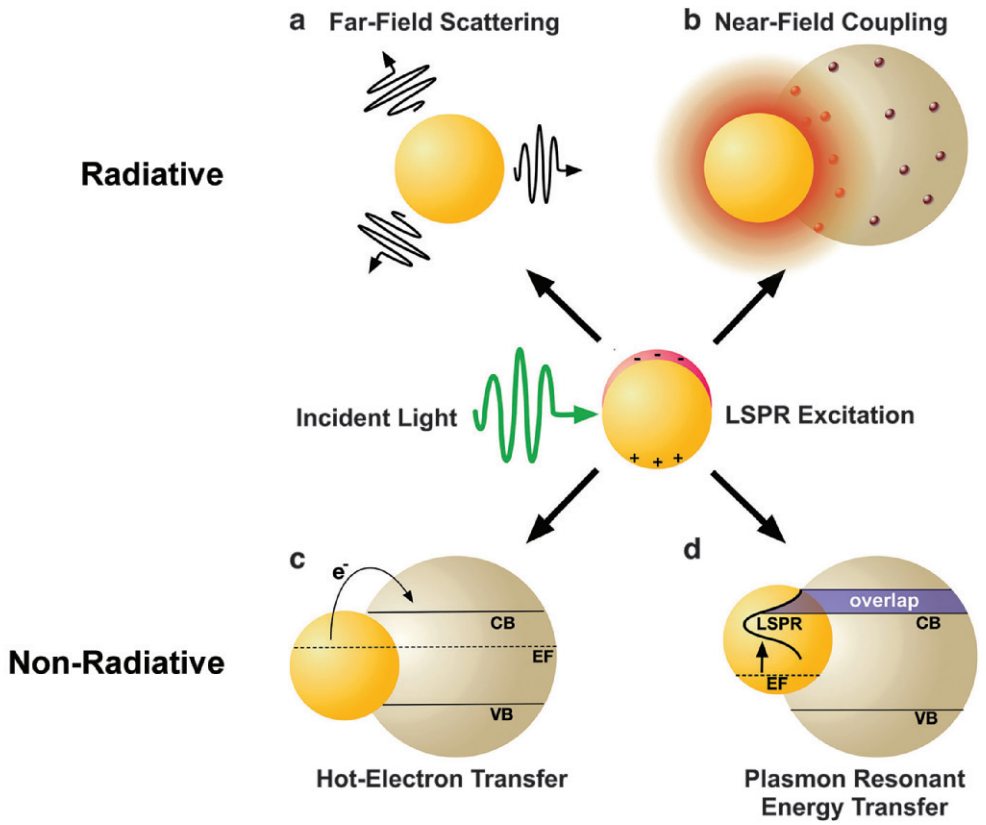

Figure 9. Schematic illustration of plasmon enhancement mechanisms: (a) far–field scattering and (b) near–field coupling (radiative effects); and (c) hot–electron transfer and (d) plasmon resonant energy transfer (non-radiative effects).[81]

The *radiative* effects are due to the emission or absorbance of photons giving rise to an increase in the electric field close to the particle surface. This results in an increased absorption "near-field" effect, or it produces light scattering from the particle, a "far-field" effect.

Plasmonic nanostructures interacting with the incident light can result in a local enhancement of the electromagnetic field close to the particle surface – the "near-field" effect. The incident light will be confined to a small spatial volume with intensities typically orders of magnitude higher than the original intensity of the incident light. The effect of this localization has been studied in Paper III. Due to this effect, plasmonic structures can be seen as secondary light sources, increasing the total photon flux and thus increasing the overall light absorption of the material. Sensitizers in close proximity to the plasmonic structures can couple with the

"near-field" effect, resulting in an increased electron-hole pair generation from the sensitizer. In the case of solar cells, this leads to a higher density of charge carriers able to move from the LUMO band of the sensitizer to the conduction band of the semiconductor, thus increasing the overall current density of the device.

Plasmonic nanostructures with a sufficiently high albedo can effectively scatter incident light into the far-field. The scattering cross-section depends on the size and shape of the material and can be an order of a magnitude larger than the physical cross-section. The sensitizer can absorb this scattered light up to several hundred nanometers from the source, thus increasing the total amount of light trapped in the material.

The *non-radiative* effects are due to electronic excitations occurring in the particle, involving a coupling of below bandgap energy to the semiconductor. This will result in two possible mechanisms with the surrounding medium: "hot-electron transfer" or "plasmon resonant energy transfer". However, when using plasmonic materials in PV devices, the radiative effects will be the dominant mechanism for efficiency enhancement. Thus, in the papers included in this thesis, only the radiative effects have been studied in more detail.

2.4.2 Tuning the optical response of gold nanoparticles

The LSPR wavelength is influenced by the nanoparticle size and shape, enabling the tailoring of the light absorption to desired wavelengths. Since also the physical and chemical properties of materials depend on their size, careful control over the preparation of these materials is needed to ensure the narrow size distribution and reproducibility.[88,89]

Colloidal gold (i.e. particles in the size range of 1–1000 nm) has been used for thousands of years for decorative purposes. In modern times, gold colloids have seen a more widespread use in electronics, sensing and catalysis. Due to the various possible applications, as well as the beneficial chemical properties of gold, there are numerous synthesis approaches to make particles with a wide selection of sizes and shapes.[90]

Generally, gold nanoparticles (AuNPs) are synthesized by chemical reduction of Au(I) or Au(III) precursors in aqueous or organic solutions in the presence of surfactants. Chemical reduction of gold is a simple process that only requires mixing of the reagents under well-controlled external conditions. These external conditions affect the final morphology of the particle. For the preparation of nanoparticles with a narrow size distribution, the nucleation step needs to be separated from the growth step in order to prevent secondary nucleation and growth.[91] There are two main approaches to do this. The first approach is the seed-mediated growth method, where preformed nanocrystal seeds are added to a growth solution, leading to a slow growth on the seed surface. This method can also be used to synthesize anisotropic particles and core-shell particles by introducing additional components or surface

directing agents in the growth solution. The other approach is the so-called hot-injection method, where a high concentration of precursor solution is rapidly injected into a hot precursor solution, leading to a fast formation of nuclei. The nucleation rate decreases quickly after the injection and growth occurs on the seed surface.

By adjusting the processing conditions, particles with different sizes and shapes can be obtained. The reaction is controlled by the strength of the reducing agent as well as the temperature, which affects the reaction kinetics. In addition to a reducing agent, the presence of a surfactant is also needed to stabilize the particles. In Figure 10, the absorption spectra of synthesized gold nanoparticles of different sizes are shown. A clear trend can be seen when increasing the particle size, the absorption peak shifts from around 520 nm for 15 nm particles up to 600 nm and beyond for ≥100 nm particles. It is worth noting that for particles smaller than 150 nm, the (near-field) absorption becomes the dominant effect, whereas for larger particles the scattering dominates. This scattering effect can be seen in the broad absorption spectrum for the 200 nm particles.

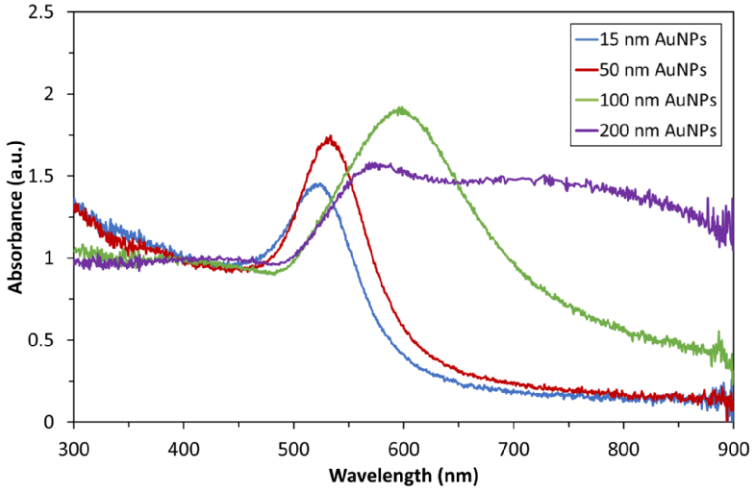

Figure 10. Absorption spectra of AuNPs with different sizes.

Most commonly, spherical AuNPs are synthesized and used. However, as previously mentioned, the overall morphology of the particles in terms of size, shape and structure influences the catalytic, electronic and optical properties. For instance, the presence of edges or tips affects the electric field enhancement. As an example of this phenomenon, by adjusting the aspect ratio (length/diameter) of gold nanorods (AuNRs), the optical response can be tuned in a wide spectral range from the visible into the NIR region. The anisotropic shape will result in two resonance peaks due to the electromagnetic radiation interacting with the surface of the particle; a transverse peak (perpendicular to the surface of the particle) and a longitudinal peak (axially along the length of the particle). By adjusting the aspect

ratio of AuNRs, the position of the transverse peak can be shifted.[92] The transverse and longitudinal peaks are discussed in greater detail in Section 5.1.2, where also absorption spectra of synthesized AuNPs of different shapes are shown.

The synthesis of anisotropic Au particles generally follows the seed-mediated growth approach as discussed earlier. In addition to separating the nucleation and growth steps, the seed-mediated synthesis also allows the seeds to influence the growth direction. For the synthesis of AuNRs, the surfactant cetyltrimethylammonium bromide (CTAB) is commonly used to stabilize the colloids and to further promote the axial growth. This is due to the preferential binding of the CTAB head group to the side crystal faces of the gold seeds compared to the faces at the tips. The presence of silver ions further promotes the AuNR growth by influencing both the yield and aspect ratio, but also the mechanism and crystal structure.[93] The preferred binding is illustrated in Figure 11.

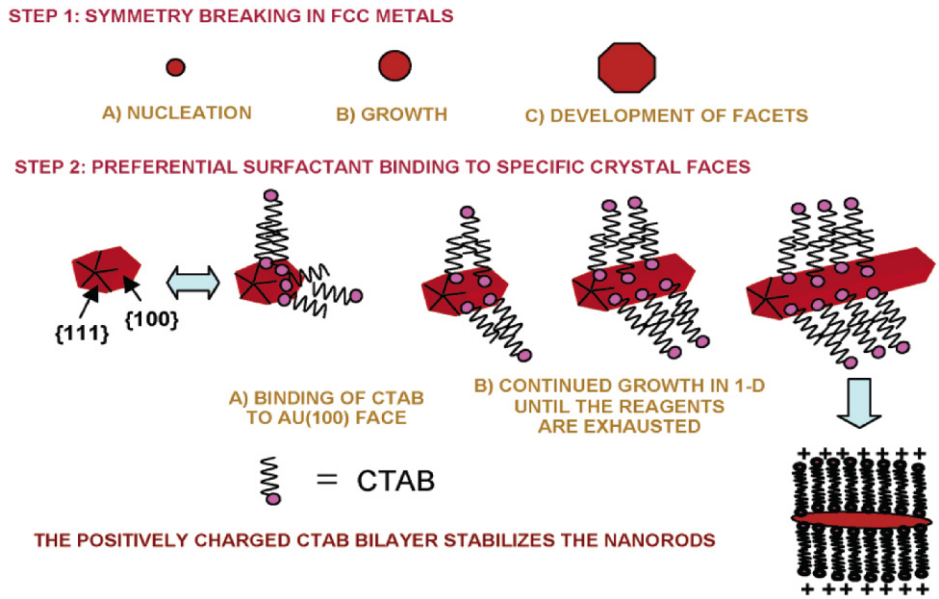

Figure 11. Illustration of the proposed mechanism for nanorod growth. The single crystalline seed particles have facets that are differentially blocked by surfactant (or an initial halide layer that then electrostatically attracts the cationic surfactant). Subsequent addition of metal ions and weak reducing agent lead to metallic growth at the exposed particle facets.[93]

The properties of nanoparticles are greatly affected by the surface functionality.[94] The surface layers influence the solubility, the stability and the electronic structure. As was previously described, surfactants are used in the synthesis procedures to stabilize the colloids and to prevent flocculation and aggregation. Molecules attached to the particle surface can also act as linkers for further functionalization and modification. Molecules can be attached either by covalent bonds or non-

covalent interactions such as physisorption or electrostatic interactions. The most common covalent approach is to utilize the strong Au-S bond by using thiol containing ligands. Other functional ligands can also be used, such as amines and phosphines, although their binding is weak and can be exchanged by thiols.

Core-shell particles are nanoparticles (the core) coated with a homogenous layer of another material (the shell). Coating the particle surface with another material is one of the most important surface treatments, since the properties of the shell can complement the properties of the core, for instance by protecting it or enabling additional functionalities. Materials such as polymers, carbon, metal and metal oxides are commonly used. The plasmonic materials used in this thesis are usually gold cores coated with a thin silica shell. A thin silica shell surrounding the gold cores serves four essential purposes: 1) it acts as an insulator to avoid charge recombination within the metal, 2) it adjusts the plasmon-dye separation distance to minimize quenching, 3) it protects the metal core from corrosion in the electrolyte solution, and 4) it improves the thermal stability, preventing sintering of the gold cores during processing.[95]

Silica (silicon dioxide, SiO_2) is one of the most widely used coating material due to its protective and stabilizing properties and well-studied chemistry.[96,97] Silica coatings are usually synthesized using sol-gel chemistry of silicon alkoxides in aqueous/alcohol solutions.[98] The thickness of the coatings as well as the porosity can be tuned by adjusting the reactants and the reaction conditions.[99] The silica surfaces can be further functionalized with amino-, mercapto- or carboxysilanes, which allows further modification and conjugation with other materials.

Although there are several approaches to produce thin silica shells on metal cores, the reproducibility of these coating protocols is not trivial due to the highly sensitive synthesis parameters (such as pH, temperature, chemical purity, etc.).[100] The so called Stöber method has been used extensively for the growth of SiO_2 nanoparticles, as well as for coating other types of particles with SiO_2 shells.[101] With this method, silica can be grown on top of gold cores to produce coatings ranging from a few nanometers up to micrometers via a sol-gel route using poly(vinylpyrrolidone) (PVP) as a coupling agent. PVP is required to enable the particle transfer to the ethanolic base solution used in the Stöber process, to improve the chemical affinity between gold and silica, and to avoid homogeneous nucleation that generates silica particles without gold cores. The major drawback of the Stöber method is the difficulty in obtaining very thin (<10 nm) silica shells in a controlled and reproducible way.

Several other methods regarding the growth of thin SiO_2 shells on AuNPs are available, but most methods follow the general route presented by Liz-Marzan et al.[102,103] In this approach, the capping ligands on the surface of the AuNPs are replaced with a monolayer of functional silane linker molecules (typically aminosilanes or mercaptosilanes) that can facilitate the affinity of silicate species on the gold surface. This process is illustrated in Figure 12.

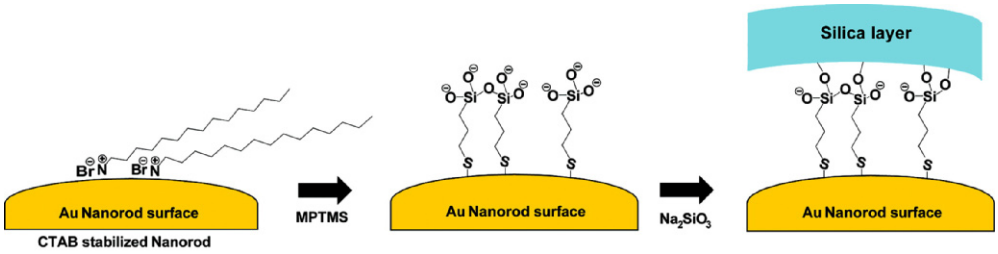

Figure 12. Schematic diagram of the surface reactions used to obtain silica-coated AuNRs.[104]

Aminosilanes can typically be used in aqueous environments, while the mercaptosilanes usually requires less reactive ethanolic conditions (i.e. a PVP coupling agent is needed). Since the semi-covalent thiol-gold interaction is significantly stronger than the electrostatic amino-gold interaction (which is also pH sensitive), a more homogeneous silane monolayer is expected when using a mercaptosilane linker.[105] After forming a monolayer on the gold surface, the siloxane groups of the linker provide excellent reaction sites for subsequent silica growth. In the syntheses, sodium silicate was used as the silica source for further growth due to its stability and moderate reactivity. By controlling the added sodium silicate amount, pH and reaction time, the silica shell can be grown to a desirable thickness. The silica shell thickness can be further increased, if needed, by a subsequent Stöber reaction step. The most crucial step in forming a thin and complete silica shell is the precise tailoring of the silica-gold interface, which requires careful control of the linking silanes to the particle surface.

2.4.3 Plasmonic solar cells

Recently, plasmonic nanoparticles have been utilized in various thin film PV technologies to enhance the overall light absorption of the PV devices.[82,83,106,107] It has been shown that spherical gold or silver nanoparticles added to the active layer can improve the performance of DSSCs,[108] organic solar cells[109] and perovskite solar cells.[110] However, the direct comparison of different studies is challenging due to the differences in the type and amount of plasmonic particles used and variation in device geometries and thicknesses. An overview regarding the different approaches in utilizing plasmonic particles in solar cells is given by Jang et al.[111] and Erwin et al.[81] When utilized in DSSCs, the plasmonic particles are usually integrated into the photoanode in order to increase the optical absorption of the sensitizer or to improve the charge transfer.[112] The amount of particles used vary between studies, but generally a positive trend in relation to the efficiency enhancement can be seen with an increasing amount of plasmonic particles integrated into the devices, levelling out at around 3 wt%.[113] The plasmonic materials used are usually bare Au or Ag nanoparticles, or core-shell particles such as Au@SiO_2, Au@TiO_2 or combinations of these with several coating layers.[114] The enhancing effects also vary significantly between different studies, from a 5% increase to four-fold increases of

the efficiencies.[115] The enhancing effects are usually attributed to an increase of the short-circuit current in the cell which is due to an increase in the light absorption of the sensitizer. Additional effects may include an increase of the short-circuit voltage or an inhibited electron recombination.[116] The large deviations in efficiency enhancements can partially be explained by the fact that these devices are typically not fully optimized devices. In many cases the effect can be difficult to properly characterize if integrated into a "standard" device structure. Additionally, many studies have not considered the chemical stability of the plasmonic materials, nor have they commented on the long-term stability of these materials in the devices.

As previously mentioned, the LSPR generated in metal nanoparticles decay either radiatively (by emitting photons) or non-radiatively (by generating electron-hole pairs). For spherical particles smaller than 50 nm, the near-field effects are dominant.[117] When using spherical nanoparticles in PV devices, the plasmon enhancement typically occurs near the generic LSPR peak of the metal used (i.e. ~400 nm for 20 nm Ag particles and ~520 nm for 20 nm Au particles). By utilizing anisotropic nanoparticles, the light absorption can be tailored to the desired wavelength (e.g. to better fit the absorption range of the sensitizer used) with adjusting the size and shape of the particle. Until now, only a few studies have used anisotropic plasmonic nanoparticles in PV applications.[118,119] The majority of these studies have failed to take into account the possible thermal deformation effects, which will dramatically influence the optical properties.

3 Aims of the study

Emerging thin film photovoltaics have a huge commercial potential due to their low-cost processing and versatile applications. Controlling the light absorption on the nanoscale in the devices is one of the key challenges, but also opens possibilities for new device structures and light management techniques. One way of controlling the light absorption is by integrating plasmonic nanoparticles into the solar cell structure. This approach requires careful control over the optical and physicochemical properties of the plasmonic particles and semiconductor materials.

The overall aim of the study was to investigate how the addition of plasmonic particles with different optical properties affect the performance of polymer- and dye-sensitized solar cells. The plasmonic particles should potentially increase the photon conversion efficiency of the solar cell and increase the spectral response of the device.

More specifically, the goal was to synthesize gold-silica core-shell particles with suitable optical properties and compatibility with the TiO_2 pastes or suspensions used for depositing the semiconducting layer of the devices. The viscosity and he addition of organic binders in the TiO_2 pastes and suspensions was adjusted to characterize their effects on the porosity and mechanical properties of the deposited TiO_2 films can be modified.

Furthermore, a study was conducted to evaluate the effect of sintering temperatures on the porosity and mechanical stability of the TiO_2 films as well as any added materials in the films. After successful integration into the devices structures, experiments were performed to investigate and model the enhancing effect of plasmonic particles on the sensitizer.

The final objective was to study the impact of the semiconductor layer thickness, as well as the particle loading, on the device properties.

4 Materials and methods

4.1 Material synthesis

In this work, AuNPs were prepared using solution-based wet chemical methods, consisting of reduction of gold salt with a reducing agent and subsequent growth of the seeds. An overview of the processing steps is given in Figure 13.

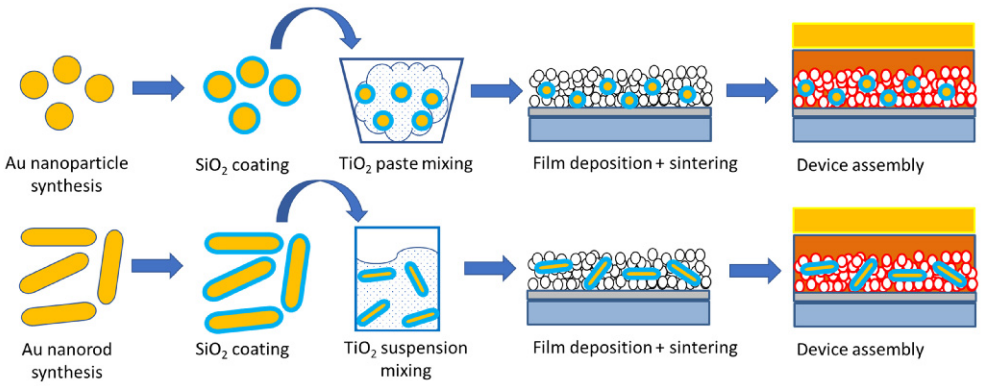

Figure 13. Workflow schematic of the material synthesis and device preparation.

The general procedure used in all studies was first the synthesis of AuNPs or AuNRs with suitable optical properties, followed by coating with a thin but homogeneous SiO_2 layer. These core-shell particles were thereafter added to a viscous TiO_2 paste or a TiO_2 suspension followed by vigorous mixing. Films were deposited on FTO substrates using screen printing or dip coating, followed by heat treatment steps. Finally, the films were sensitized and the obtained photoanodes were assembled into DSSC devices.

4.1.1 Au@SiO_2 nanoparticles

Gold-silica core-shell nanoparticles (Au@SiO_2 NPs) were synthesized using wet chemical methods. The AuNP cores were synthesized according to the method by Turkevich et al.[120] An aqueous solution of gold (III) chloride hydrate ($HAuCl_4$) was brought to boil. Sodium citrate, acting as both a reducing agent and as a stabilizer, was added and the solution was left to boil for 30 min. The solution turned from light yellow to ruby-red in a few minutes, indicating the formation of citrate-capped AuNPs. In order to improve the nanoparticle stability in non-aqueous solutions, the capping agent must be exchanged. Thus, an aqueous solution of PVP was added to the AuNPs under vigorous stirring. The solution was left to react for 24 h under stirring, thereafter centrifuged and washed with water.

Several methods for forming a protective and insulating SiO_2 shell on the AuNP surfaces were studied. An overview of the methods is given in Figure 14. First, a monolayer of functional silanes, i.e. (3-aminopropyl)trimethoxysilane (APTMS) and (3-mercaptopropyl)trimethoxysilane (MPTMS), were coated on the particles. The silanes were added to the aqueous (APTMS, APTMS+Stöber, Stöber methods) or ethanolic (MPTMS method) AuNP solutions and stirred for 20 min. The silanes act as linkers to the particle surface and allow for subsequent silica growth on the surface. An aqueous sodium silicate solution was added to the silane-modified AuNPs, stirred for 20 min and allowed to stand for 12 h undisturbed, forming a silica shell around the particle. The shell thickness can be adjusted by modifying the reaction time for the shell growth. The use of APTMS with a subsequent sol-gel Stöber growth was studied as a method of increasing the thickness of the surface coating. As a comparison, a direct Stöber growth without any linking molecules on the particle surface was investigated.

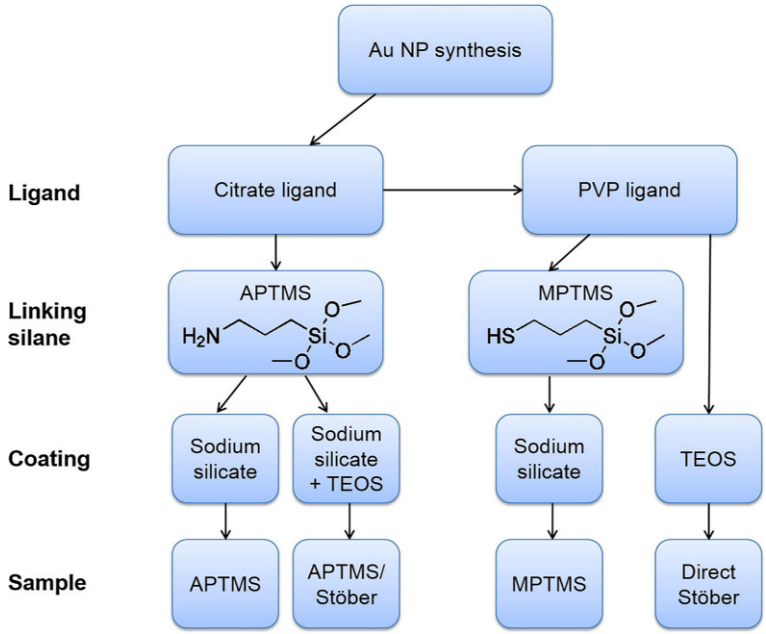

Figure 14. Flowchart of the Au@SiO_2 NP synthesis methods used in this work.

4.1.2 Au@SiO_2 nanorods

AuNRs were synthesized following the two-step method presented by Nikoobakht and El-Sayed.[121] First, a gold seed solution was first prepared by mixing an aqueous CTAB solution with $HAuCl_4$ under stirring. The gold salt was reduced by adding sodium borohydride ($NaBH_4$), turning the solution from light yellow to brownish yellow, indicating the formation of gold seeds. Growth solutions were prepared by adding an aqueous CTAB solution to a varying amount of silver nitrate

($AgNO_3$) solution. The amount of $AgNO_3$ controls the AuNR aspect ratio; the aspect ratio will increase with increasing $AgNO_3$ content. Thereafter, $HAuCl_4$ was added to the growth solution and reduced with the addition of ascorbic acid. The growth solution changed color from dark yellow to colorless, indicating the reduction of the gold ions. Ascorbic acid is a weak reducing agent for gold and thus particles cannot be formed; only change the oxidation state of the gold. Finally, the seed solution was added to the growth solution. The samples gradually changed color during the first 15–30 min, resulting in a dark brown color. This method provides AuNRs with aspect ratios up to five with high yield and fairly good uniformity. In this thesis, low aspect ratio AuNRs with an aspect ratio of 1.7 and wavelength at 700 nm, and high aspect ratio nanorods with an aspect ratio of 3.2 and wavelength at 800 nm were produced. In the gold-silica core-shell nanorods (Au@SiO_2 NRs), a thin SiO_2 layer on the particle surface was synthesized with the MPTMS linker and growth with sodium silicate, as described in Section 4.1.1.

4.1.3 Metal oxide pastes/suspensions

The plasmonic core-shell particles were incorporated into the photoanode by dispersing/mixing them into a TiO_2 paste/suspension, which was thereafter deposited onto FTO glass and sintered.

In order to make a paste for screen printing the photoanodes, a modified version of the method presented by Ito et al. was followed.[122] TiO_2/Au@SiO_2 paste was prepared by mixing 0.1 g Aeroxide P25 TiO_2 nanoparticles, 0.4 g α-terpineol, 0.033 g ethyl cellulose, 0.01 g Au@SiO_2 NPs and 0.1 g ethanol. The mixture was vigorously shaken for a day to ensure homogeneity and excess solvent was then evaporated to achieve the proper viscosity. Reference standard TiO_2 paste without Au@SiO_2 NPs was also prepared in a similar way.

A TiO_2 suspension suitable for low-temperature processing was prepared following a modified method based on Zhang et al.[123] and Kim et al.[124] P25 TiO_2 nanoparticles were pre-heated to 450 °C to remove any organic contaminants and absorbed moisture. A suspension of TiO_2 nanoparticles was prepared by mixing 1 g of P25 TiO_2 with 8.5 g of ethanol and 0.14 g of deionized water. This suspension was sonicated with a 50 W sonic horn (Vibra-Cell 50AT, Sonics & Materials Inc.) for 30 min. To this suspension 0.36 g of titanium isopropoxide was added and mixed with a magnetic stirrer for 4 h to ensure homogeneous mixing. During the preparation, Au@SiO_2 NRs dispersed in ethanol were added to the suspension corresponding to 2 wt% of the final film composition.

4.2 Film deposition

4.2.1 Screen printing

Screen printing is a stencil printing technique utilizing a mesh screen to regulate the dimensions of the deposited film. A viscous paste is pushed through a wire mesh using a rubber squeegee. The film dimensions are regulated by the screen size, while the thickness is controlled by the paste properties and the mesh openings. Usually the pastes are viscous, and the films are formed in the micrometer range. The screen printing was carried out using a SCF-260B screen printer (Technical Industrial Company, China). The TiO_2 pastes with/without $Au@SiO_2$ NPs were thereafter deposited onto FTO glass using screen printing followed by heat treatment at 500 °C for 30 min to remove the organic components in the paste and to ensure sufficient particle connectivity and stability in the mesoporous structure.

4.2.2 Dip coating

In the dip coating process, the substrate is immersed into a solution and withdrawn vertically at a constant speed. Due to the drag from the moving substrate, a thin liquid film will remain on the surface as it is withdrawn from the solution. The solvent evaporates, and the non-volatile species remain on the substrate. The film thickness is determined by the withdrawal rate and viscosity, and the density of the solution. The dip coating used in this study was carried out with a KSV Dip Coater (Biolin Scientific, Sweden). TiO_2 films with or without $Au@SiO_2$ NRs were prepared by dip coating the suspension four times onto FTO glass substrates, with a heat treatment at 120 °C for 10 min after each dip. The films were thereafter sintered at 200 °C for 30 min.

4.3 Device manufacturing

The sintered TiO_2 films were immersed in solutions containing sensitizers, forming the photoanodes. The sensitizer used in Papers I and II was the Ru-complex N719 (*cis*-diisothiocyanato-bis(2,2'-bipyridyl-4,4'-dicarboxylato) ruthenium(II) bis(tetrabutylammonium)), and the sensitizer used in Paper III was a partially hydrolyzed copolymer PT-C 85 (poly[(methylthiophene-3-yl-carboxylate)-ran-(thiophene)]).[125] The molecular structures of the sensitizers used are shown in in Figure 15.

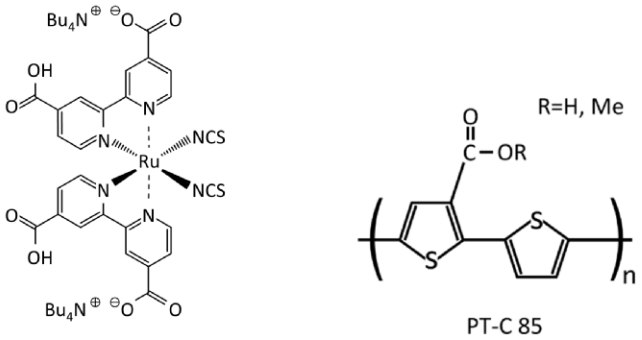

Figure 15. Molecular structure of N719 dye and PT-C 85 polymer.

Photoanodes were made by immersing the films in a dye solution containing 3 mM of the ruthenium dye N719 in a mixture of acetonitrile/*tert*-butyl alcohol for 20 h. Photoanodes using the polymer as a sensitizer were prepared by immersing the sintered TiO_2 films into a 0.1 mg/ml solution of PT-C 85 in dimethyl sulfoxide for 20 h to form a thin homogeneous polymer layer on the mesoporous TiO_2 structure.

DSSCs based on the N719 dye were assembled by sandwiching thermoplastic ionomer spacer films between the photoanodes and Pt-coated FTO glass substrates and injecting the liquid electrolyte (0.1 M lithium iodide, 0.6 M 1,2-dimethyl-3-propylimidazolium iodide, 0.5 M 4-*tert*-butylpyridine, 0.025 M iodine in acetonitrile) between them. The polymer-sensitized solar cell (PSSC) was assembled by sandwiching spacer films between the photoanodes and a Pt-coated FTO glass and injecting a liquid I^-/I_3^- electrolyte (0.5 M tetra-n-butylammonium iodide, 25 mM I_2 in acetonitrile) between the electrodes.

4.4 Characterization methods

4.4.1 Material characterization

4.4.1.1 Ultraviolet-visible spectroscopy

One of the most common techniques for studying the optical properties of nanomaterials is UV-vis spectroscopy. The basic principle of electronic absorption spectroscopy is the measurement of light absorption due to electronic transitions in the sample.[126] The relation of the attenuated light to the material properties and the concentration is described by the Beer-Lambert law[127]:

$$A = log_{10}\frac{I_0}{I} = \varepsilon lc$$

In the equation, A is the sample absorption, I_0 and I are the intensities of light passing through the reference and the sample cell, respectively, ε is the molar absorption coefficient, l is the path length and c is the concentration. The intensity

of the transmitted light can be plotted as a function of light wavelength, giving an absorption spectrum.

In the case of thin films, the optical effects will be a combination of transmittance (T), reflectance (R), and absorption (A) according to the following relation[128]:

$$T + R + A = 1$$

When a focused light beam passes through a thin film, the beam will lose intensity due to scattering and absorption. If the roughness of the film is high, the reflectance will be dominated by the diffuse reflectance, i.e. the light is reflected in all angles equally or near-equally. Thus, in many cases it is useful to look at the absorptance (k) of a sample:

$$k = \frac{100 - T - R}{100}$$

The UV-vis spectrometer used to characterize liquid samples was a UV-2501PC (Shimadzu, Japan), and a Lambda 900 (PerkinElmer, USA) with a PELA-1020 integrating sphere setup was used to characterize films in this study.

The transmittance and total reflectance of the films were measured with the light beam at 0° incidence to the surface of the film. A mask was used to limit the measurement beam only on the TiO_2 film and minimize the effect of reflection from the substrate and film edges.

4.4.1.2 Electron microscopy

Optical microscopes have limited resolution due to the diffraction limit of light. However, for studying nanomaterials higher resolution is needed. The most common electron microscopy methods for characterizing nanomaterials are scanning electron microscopy (SEM) and transmission electron microscopy (TEM). For both methods, the operating principle is based on the use of accelerated electron beams, generating scattered electrons from the surface or transmitted electrons passing through the sample. The signal from the scattered and unscattered electrons can be gathered by a detector, creating an image of the sample.

In an SEM, the electron beam is scanned across the sample surface. The electron beam interacts with the surface atoms, creating electron emissions from the surface. The backscattered or secondary electrons emitted are detected by the SEM, giving information about the sample surface.[129] Generally, SEM has a lower resolution than TEM. However, the samples measured can be thicker since the electron interaction takes place at the surface.

A TEM has a high spatial resolution close to 0.1 nm, and is capable to obtain information about particle size, shape, crystallinity, and interparticle interaction.[130] The operating principle is similar to SEM; the major difference is that a TEM operates at a higher acceleration voltage and can detect transmitted electrons. A

TEM instrument can also provide crystallographic information about the sample. In crystalline specimens, the electrons are scattered in very distinct directions due to the crystal structure; thus, causing a diffraction contrast in the image. A diffraction pattern will be formed at a point below the objective lens known as the back focal plane. By varying the strengths of the lenses immediately below the objective lens, it is possible to enlarge the diffraction pattern and project it onto the viewing device.

The SEM used in the studies was a Leo 1530 Gemini (Zeiss, Germany). The TEM instruments used were a Tecnai 12 Bio-Twin (FEI Company, USA) operating at 120 kV and an Tecnai F20 (FEI Company, USA) operating at 200 kV.

4.4.1.3 Atomic force microscopy

An atomic force microscope (AFM) is a high-resolution type of scanning probe microscope with a spatial resolution in the nanometer range. An AFM consists of a flexible cantilever with a sharp tip (probe) at its end that is used to scan a sample surface. When the tip is brought into close proximity of a sample surface, the repulsive or attractive forces between the tip and the sample lead to a deflection of the cantilever. The deflection of the cantilever is monitored with a laser beam and a photodiode detector.

By monitoring the change in the cantilever deflection while scanning over the sample surface, a 3D image of the surface can be obtained. Several imaging modes can be used when imaging a sample: contact, non-contact and tapping modes.[130] In the contact mode, the cantilever tip makes physical contact with the sample surface, deflecting the cantilever. However, due to the direct physical contact, there is a risk of deforming the tip or the sample surface. In the non-contact mode, the tip hovers above the sample, and attractive forces between the tip and sample are measured. The main drawback is that the forces measured are much weaker than in the contact mode. Tapping mode combines the advantages of the previous modes, by oscillating the tip and briefly tapping the surface. This has the advantage of achieving a high resolution without inducing damaging forces.

The AFM used for the studies was an Ntegra-Prima (Spectrum Instruments Limited, Ireland).

4.4.1.4 Scanning white light interferometry

Scanning white light interferometry (SWLI) is a measurement technique that provides a non-contact and non-invasive 3D method for measuring surface roughness as well as imaging surfaces.[132]

A beam splitter separates light from a white light source into two separate beams. One beam is directed towards the sample and one beam is directed towards an internal reference mirror. The two beams are reflected or scattered from their respective surfaces. The reflected light beams recombine, and the recombined light is sent to the detector. When the path length to the sample and the reference are the same, interference is observed. By changing the path length of the measurement

beam relative to the reference beam, a correlogram of the interference is generated. The z-value for a point on the surface corresponds to the z-value of the positioning stage when the modulation of the correlogram is the greatest. This results in a series of images of the intensity, which are used to characterize the surface being measured. White light is used rather than monochromatic light because it has a shorter coherence length that results in a greater accuracy. The accuracy and repeatability of the scanning white light measurement are dependent on the control of the scanning mechanism and the calculation of the surface properties from the interference data.[133]

The samples in this study were measured using a custom-made SWLI instrument and analyzed using the MountainsMap® Imaging Topography 7.1 software.

4.4.1.5 X-ray diffraction

X-ray diffraction (XRD) is a non-destructive x-ray technique used to determine structural features such as the atomic and molecular arrangement of crystalline materials. The crystalline sample is radiated at selected orientations with a monochromatic x-ray beam.

Due to the periodic crystal structure, a constructive interference occurs in certain directions fulfilled by Bragg's Law[134]:

$$2dsin\theta = n\lambda$$

In the equation, the d is the spacing between diffracting planes, θ is the scattering angle, n is an integer and λ is the wavelength of the beam.

When the sample or the detector is moving, the x-rays will diffract at certain angles, thus giving a diffraction pattern (diffractogram) from the scattered beams. The diffractogram is a plot of the scattered x-ray intensity versus the detector angle. The positions of the reflections depend on the arrangement of unit cells and lattice spacing in the material, and therefore the diffraction pattern is unique for different materials. The obtained diffractogram can be used to determine the crystal structure, crystal phase, and distances between scattering planes (d-spacing) of the material.

The XRD measurements in this study were carried out using a AXS D8 Discover (Bruker, USA) using a Cu K_α x-ray source.

4.4.2 Device characterization

4.4.2.1 Current-voltage measurements

The overall solar energy to electrical energy conversion efficiency, η, is given by the following equation, where J_{sc} is the short-circuit current, V_{oc} is the open-circuit voltage, P_{in} is the intensity of the incoming light and FF is the fill factor:

$$\eta = \frac{J_{SC} V_{OC} FF}{P_{in}}$$

The *FF* can theoretically assume values between 0 and 1 and is defined by the following equation, where P_{max} is the maximum power, which is obtained from the product of the photocurrent and photovoltage, where the power output of the cell is at its maximum:

$$FF = \frac{P_{max}}{J_{SC} V_{OC}}$$

The current-voltage (I-V) characteristics of the DSSCs were measured under AM 1.5G irradiation at 100 mW/cm^2 using a Xe lamp solar simulator PEC-L01 (Peccell, Japan).

4.4.2.2 Incident photon to current conversion efficiency measurements

Another method to characterize the performance of a solar cell is to measure the so called "external quantum efficiency" or, alternatively, the IPCE. The IPCE value corresponds to the photocurrent density in the solar cell produced under monochromatic illumination divided by the photon flux striking the cell. The IPCE as a function of wavelength can be calculated from the following formula:

$$IPCE = \frac{J_{SC}(eV)}{e\Phi(eV)} = 1240 \frac{J_{SC}(\lambda)}{\lambda P_{in}(\lambda)}$$

In this case, the e is the elemental charge and Φ is the light flux. The conversion factor from electron volts (eV) to nm (λ) is 1240. IPCE values provide information about the wavelength dependent quantum efficiencies of the solar cell.

The IPCE spectra were measured with QEX7 measurement system (PV Measurement Inc, USA) with a monochromator equipped with a 150 W Xe lamp.

5 Results and discussion

In this thesis, the design of plasmonic materials for solar cell applications was investigated and their effect on the performance of DSSC devices was studied. When incorporating plasmonic materials in DSSC devices, several crucial factors need to be considered. The plasmonic materials need to be designed with suitable optical properties matching that of the active material in the device. The materials should withstand the applied processing conditions and the environment in the cells without deformation or dissolution. Furthermore, the materials should have a minimal negative impact on the device performance, i.e. they should not affect the charge mobility or quench the charge carriers.

5.1 Plasmonic nanoparticles

5.1.1 Core-shell structure

In Paper I, four different methods for preparing thin silica coatings on AuNPs were studied. The methods were based on either aminosilane or mercaptosilane linking chemistries, and/or the Stöber sol-gel process. These approaches gave rise to thin silica coatings ranging between 1–20 nm in thickness. An overview of the synthesis methods and steps was given in Figure 14 in Section 4.1.1.

The AuNPs were prepared according to the well-established method presented by Turkevich et al.[120], forming 15–20 nm spherical Au particles. The linking silanes (APTMS and MPTMS) were used to coat the particles before growing thicker SiO_2 shells with sodium silicate. The use of APTMS with a following sol-gel Stöber growth was also studied as a method of increasing the thickness of the surface coating. As a comparison, a direct Stöber growth without any linking molecules on the particle surface was also studied.

The core-shell structures of the particles were studied using TEM. The images are shown in Figure 16. The spherical Au cores in all samples had a relatively homogeneous size of 16.4 ± 1.4 nm in diameter illustrating that none of the coating methods affected the Au cores. It appeared that the APTMS method did not result in a homogeneous coating, as both coated patches (~4 nm thick) and non-coated particle surfaces can be seen in Figure 16a. The method using APTMS with a subsequent Stöber reaction step gave a more homogeneous surface with an around 3 nm thick coverage (Figure 16b). The coating method using MPTMS as a linker molecule also resulted in a similar homogeneous ~5 nm thick coating (Figure 16c). The direct Stöber coating of the particles also gave a homogeneous coating, although the silica thickness was increased to about 7 nm (Figure 16d). However, a large amount of homogeneously nucleated silica by-products could also be seen in this sample (highlighted in the inset in Figure 16d). The incomplete coverage observed

for the APTMS method is most likely due to the relatively weak coordination of amines to the gold surface, which can lead to disorder at the core-shell interface and thus affect the subsequent shell formation. By contrast, the method using the mercaptosilane MPTMS as linker gave a homogenous and thin silica coverage without the need for additional growth steps. The thiol-gold interaction is very strong and leads to an ordered monolayer at the core-shell interface which improves the shell formation. It is worth noting that the coating process itself is very sensitive to small fluctuations in the synthesis conditions, possibly affecting the reproducibility of the used coating protocol.

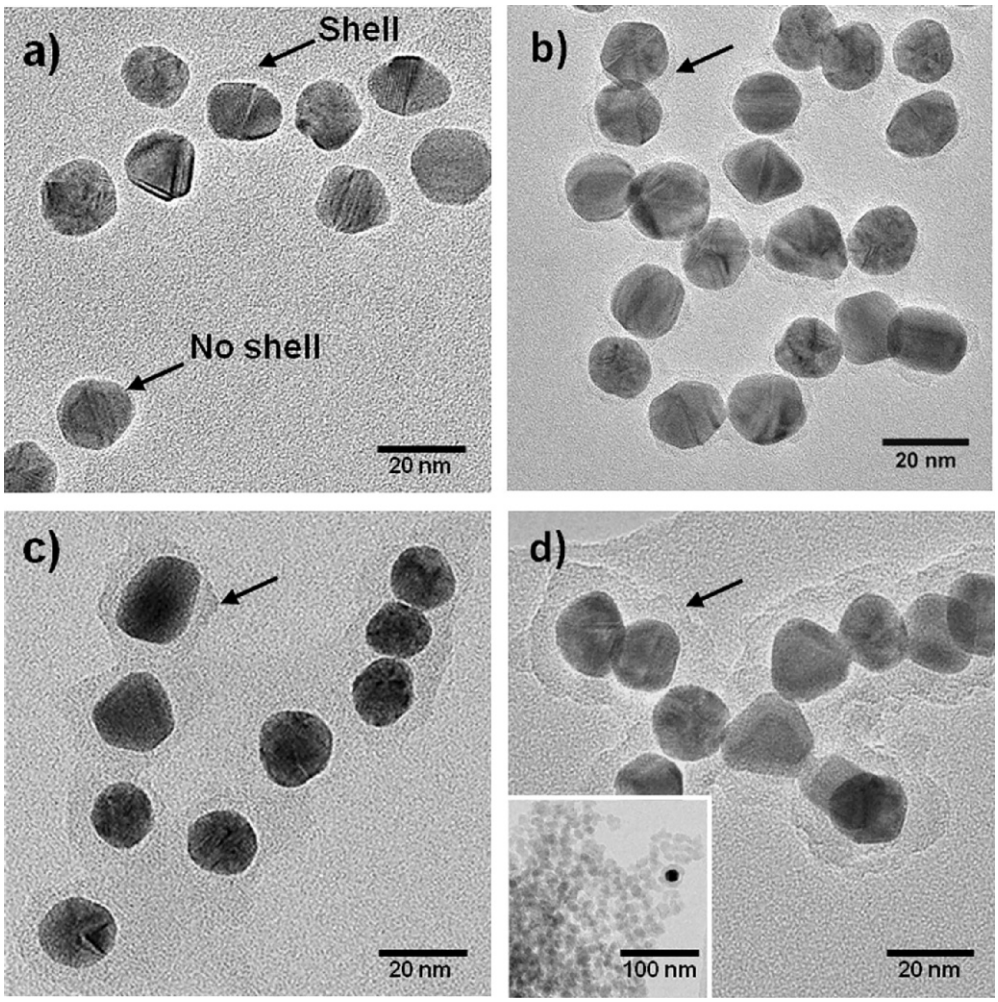

Figure 16. TEM images of synthesized core-shell particles: a) APTMS, b) APTMS/ Stöber, c) MPTMS, and d) Direct Stöber (inset shows a lower magnification of the Direct Stöber sample).

In Paper II, AuNRs with different aspect ratios were synthesized and coated with a thin SiO_2 shell using the method with MPTMS linking silane, as investigated in Paper I. The TEM images in Figure 17 show uncoated AuNRs with aspect ratios of around 1.7 (Au NR-1) and 3.2 (Au NR-2) as well as a core-shell particle with a thin SiO_2 shell. The MPTMS coating method, as presented in Paper I, was used for the silica coating of all gold samples.

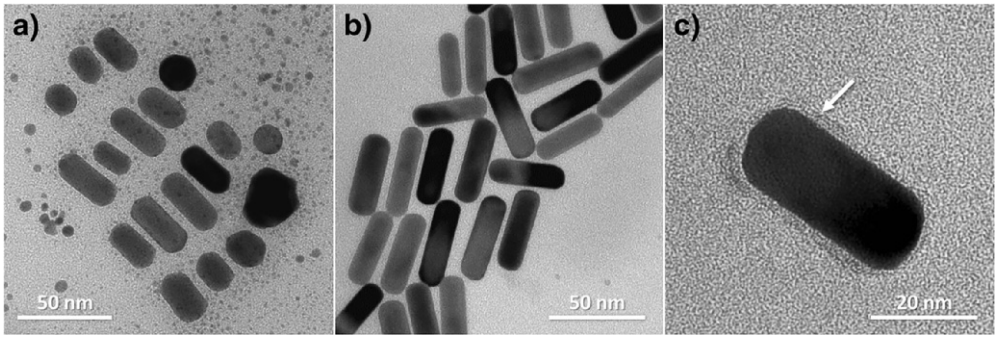

Figure 17. TEM images of the two AuNR samples used in Paper II: a) Au NR-1, b) Au NR-2, and c) the thin SiO_2 coating for the Au@SiO_2 NR-1 sample.

5.1.2 Optical properties

The optical properties of plasmonic nanoparticles depend on their size, shape, and the surrounding medium. This is illustrated in Figure 18, where UV-vis absorption spectra on different size AuNPs and different aspect ratio AuNRs are shown.

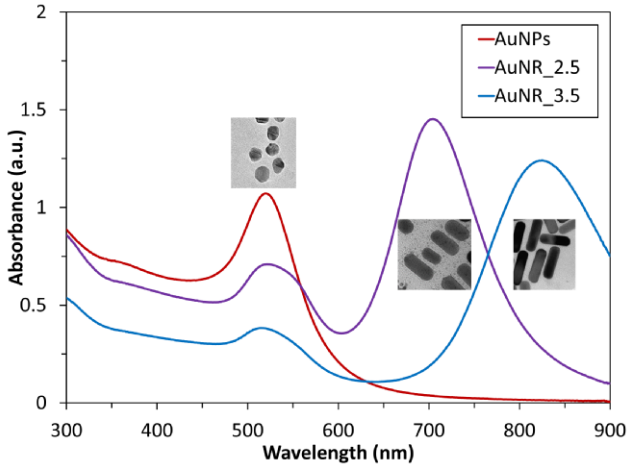

Figure 18. Absorption spectra of AuNPs of different shapes: Spherical AuNPs (red); AuNRs with aspect ratio 2.5 (purple); AuNRs with aspect ratio 3.5 (blue).

Furthermore, coating the particles with a thin SiO_2 shell (Papers I–III) shifted the absorption maxima of the peaks due to a change in the dielectric constant of the medium surrounding the particles. This shift can be seen in Figure 19, where UV-vis spectra of core-shell particles with different shell thicknesses are shown. However, this effect is very minuscule for thin layers, so the resulting shift remained quite small. The results from the UV-vis measurements can be compared with the extinction absorption coefficient Q_{abs} calculated using the Mie theory. The modeling of the red-shift in the UV-vis data resulted in a thinner silica shell (~1.5 nm) when compared to the thickness observed in the TEM image (~5 nm). The MPTMS sample gave a smaller silica thickness of ~1.5 nm when modeling the red-shift in the UV-vis data. The Stöber sample, on the other hand, resulted in a much larger silica thickness of 20–50 nm compared to the ~7 nm observed by TEM. It should be noted that the UV-vis method is a bulk method and should give more reliable values than the thicknesses obtained from the TEM measurements where only a few particles are examined.

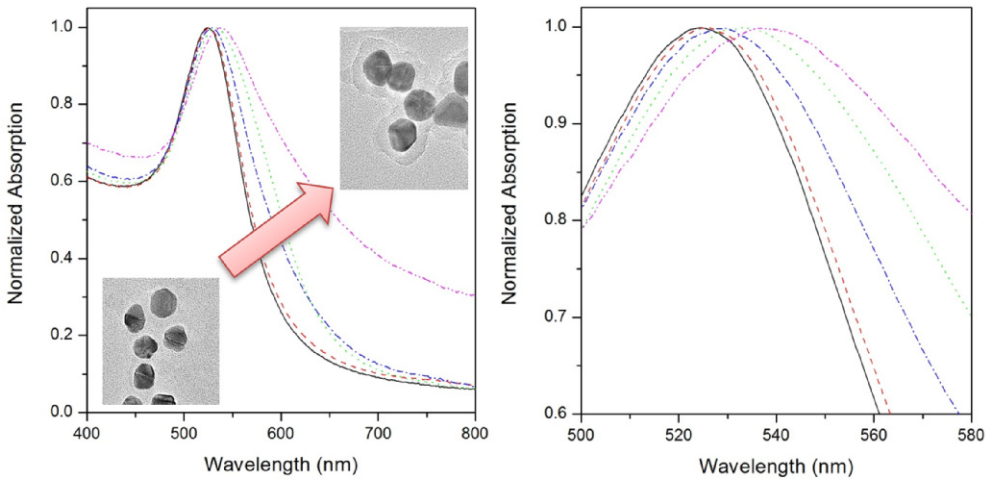

Figure 19. UV-vis spectra of AuNPs with different silica shell thickness.

5.1.3 Chemical stability

As was mentioned in Section 2.3.1, the I^-/I_3^- liquid electrolyte commonly used in DSSCs is chemically very aggressive against noble metals, so the plasmonic particles must have a sufficiently thick protective coating in order to prevent rapid dissolution. In Paper I, the chemical stability of the synthesized $Au@SiO_2$ NPs against the liquid electrolyte was studied using optical methods. The core-shell particles were dispersed in acetone and a drop of electrolyte containing the I^-/I_3^- redox couple was added. Particles with an incomplete silica coating (sample APTMS) dissolved within minutes, which could be observed visually by a change from the characteristic purple color of the colloidal plasmonic particle dispersion

to a light yellow color characteristic of the Au^{3+} ions (Figure 20a). When adding electrolyte to the other samples with complete SiO_2 coatings, the particles started to flocculate and sediment rapidly after the addition of the electrolyte solution. However, the particles were easily redispersed by ultrasonication and retained their characteristic light purple color (Figure 20a). Importantly, this implies that gold cores were protected against the aggressive electrolyte. The flocculation might occur due to charge screening of the particle surface charges as a result of adsorption of the cationic species in the electrolyte solution, thus leading to (reversible) aggregation. Furthermore, the dissolution kinetics of the incompletely coated samples was studied in more detail by measuring absorption spectra on the solution before and at regular intervals after the addition of electrolyte (Figure 20b). A rapid decrease of the plasmonic gold peak at 525 nm could be seen almost immediately, and after 5 min the plasmonic peak had almost completely disappeared, confirming the visual observations. These results indicate that a complete silica coating is crucial in order to successfully incorporate gold nanomaterials in liquid electrolyte DSSCs.

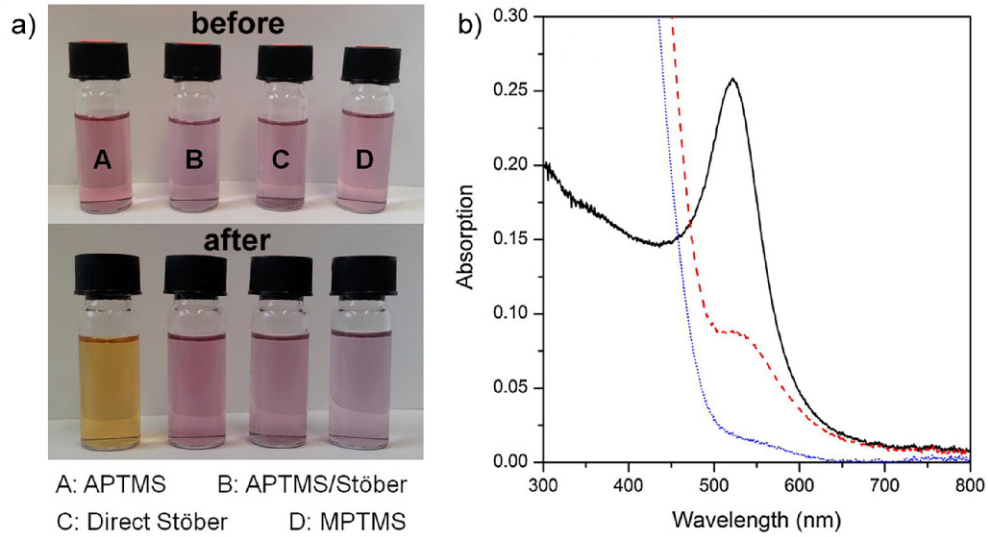

Figure 20. a) Picture of core-shell Au particles dispersed in acetone before and after electrolyte addition and b) UV-vis spectra of the APTMS sample before (–––) and after electrolyte addition: 1 min (-----) and 5 min (·····).

5.1.4 Thermal stability

It has been shown that the chemical stability is crucial when incorporating core-shell nanoparticles into the photoanodes used in DSSC applications. Additionally, they also need to be able to withstand the thermal treatment when sintering the deposited films. The particles should not deform during such processing steps, as this also affects their optical properties. The SiO_2 coating should also not crack or deform at these elevated temperatures, which potentially could lead to the

dissolution of the gold cores when the electrolyte solution is introduced at the DSSC assembly stage.

5.1.4.1 Spherical particles

To study the effect of the heat treatment, the core-shell particles coated by the MPTMS method were monitored using a high-resolution TEM with an *in situ* heating holder. Images were taken before and after heating to 500 °C. From the images shown in Figure 21, good thermal stability of the core-shell particles can clearly be seen; there are only marginal restructuring and sintering effects. No cracking or deformation of the silica shell was observed, and the particles in close proximity were not merged with each other.

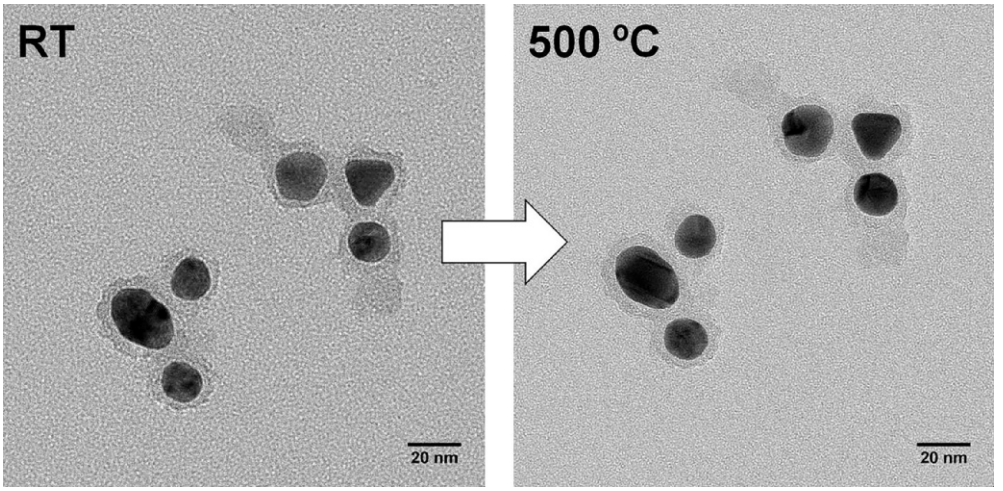

Figure 21. TEM images of Au@SiO_2 NPs (MPTMS method) at room temperature and at 500 °C.

5.1.4.2 Anisotropic particles

In most plasmonic applications, spherical nanoparticles have been used because of the relatively easy synthesis and their good colloidal stability in suspensions. However, anisotropic particles such as AuNRs would offer a larger flexibility in device design due to their unique optical properties, as has been explained previously in Section 2.4.2. However, a major issue regarding the utilization of anisotropic plasmonic nanoparticles is their low thermal stability.[135] At elevated temperatures, their structure starts to deform in order to lower the overall surface energy (i.e. the nanorods become more spherical). This deformation will change the aspect ratio of the particles and influence the absorption wavelength.

In Paper II, the deformation of Au@SiO_2 NRs as a function of sintering temperature was investigated. The effects of thermal treatment on the core-shell particles were first studied optically by drop casting the colloidal solutions on glass slides and heating the samples to different temperatures. Absorption spectra of

Au@SiO_2 NR samples heated to different temperatures are shown in Figure 22. No substantial effect on the longitudinal plasmonic peak up to 200 °C could be seen, the peak maximum remained fixed at ~700 nm. This indicates that the nanorods can be considered thermally stable up to this temperature. However, at higher temperatures the longitudinal peak started to shift towards lower wavelengths and finally merging with the transversal peak into one broad peak, indicating that the particles become more spherical.

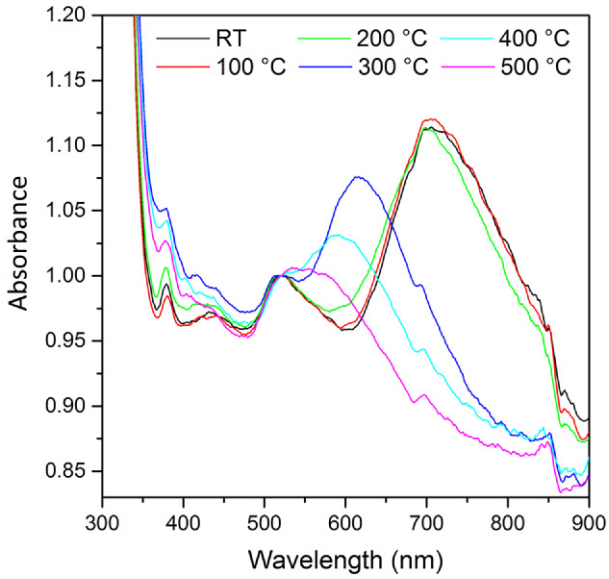

Figure 22. UV-vis absorption spectra of AuNRs heated to different temperatures.

This deformation was further confirmed by TEM measurements using *in situ* heating (Figure 23). At lower temperatures the nanorods were stable with minimal structural changes. However, at temperatures higher than 200 °C the nanorods started to deform. This restructuring occurs to reduce the interfacial energy and results in a lowering of the particle aspect ratio (and ultimately fusing of the particles). This deformation and change of optical properties at elevated temperatures were in good agreement with previous studies on bare AuNRs.[120,136]

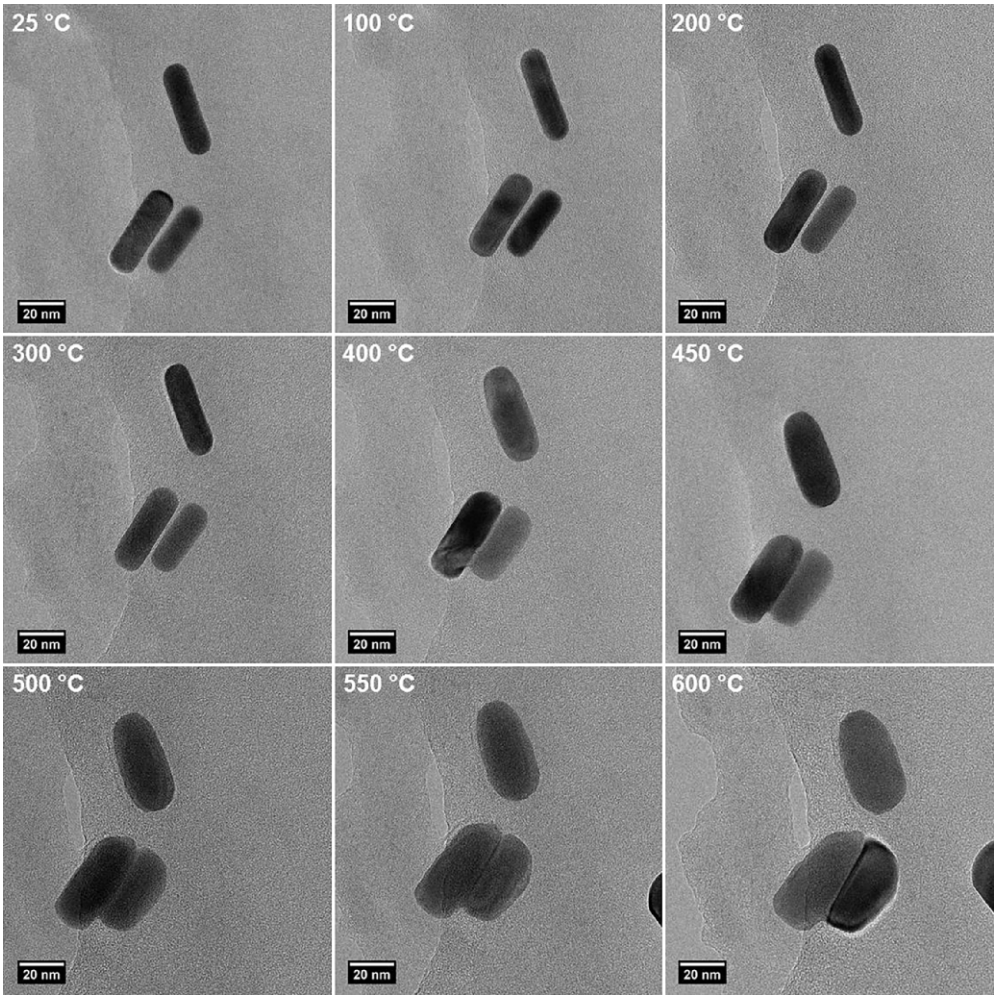

Figure 23. TEM images of Au@SiO_2 NRs at increasing temperatures.

Based on the TEM images, the change in the aspect ratio as a function of temperature was analyzed (Figure 24). A small decrease in the aspect ratio with increasing temperature can be seen up to 300 °C, while at higher temperatures a rapid and more drastic deformation is evident. Thus, to minimize deformation and to fully utilize the Au@SiO_2 NRs in DSSC applications, all processing steps must take place at relatively low temperatures (i.e. 200 °C or below). This is significantly lower than the commonly used sintering temperatures for TiO_2 photoanodes in DSSCs (i.e. ~500 °C).

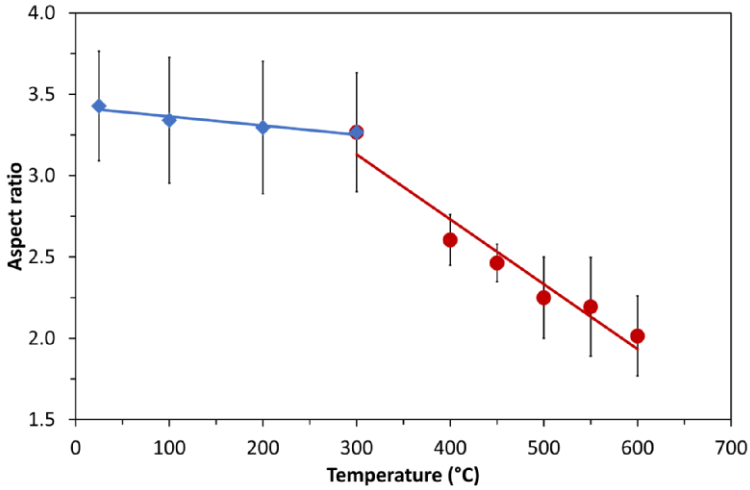

Figure 24. Change in AuNRs aspect ratio versus temperature with linear regression fits before (blue) and after (red) the critical deformation temperature.

5.2 Plasmonic particles in TiO_2 films

The addition of plasmonic particles to the photoanode in DSSCs must also have a minimal impact on the structural and electronic properties of the semiconductor film. In Figure 25, SEM images of TiO_2 films deposited by screen printing or dip coating are shown. It is evident that the screen printing pastes produced more porous films, most likely due to the presence of organic binders in the paste, whereas the dip coating suspensions produced more dense films. The addition of plasmonic particles into the screen printing pastes (Paper I and III) did not affect the structure or processing properties of the TiO_2 films. However, for photoanodes, which were manufactured using dip-coating followed by low-temperature processing (as required for anisotropic particles used in Paper II), the addition of plasmonic particles had a much larger effect on the structure, increasing the surface roughness and changing the porosity of the films.

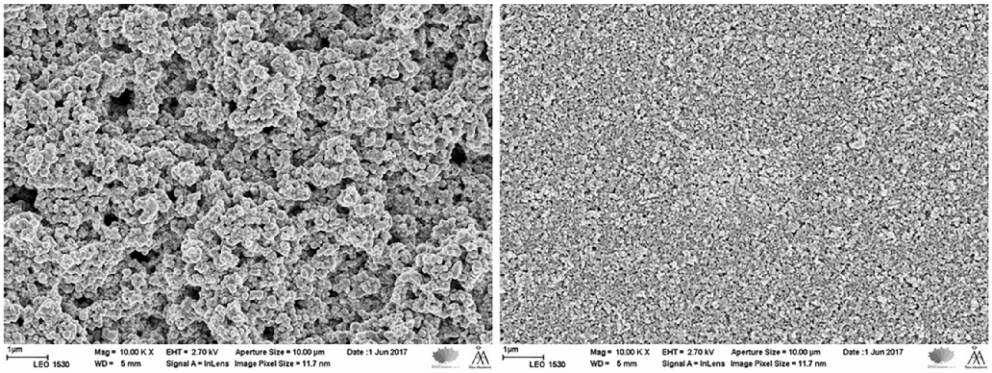

Figure 25. SEM images of TiO_2 films deposited from screen printing pastes (left) and dip coating suspensions (right).

5.2.1 Screen printing pastes

In Papers I and III, the plasmonic core-shell particles were incorporated into viscous pastes consisting of TiO_2 with ethyl cellulose and terpineol as binders. These pastes were deposited on substrates using screen printing and were subsequently sintered at 500 °C. The incorporation of particles had minimal effect on the structure and performance of the films.

5.2.2 Dip coating suspensions

In Paper II, a TiO_2 paste suitable for low-temperature processing at 200 °C was developed. Films were deposited by dip coating of TiO_2 suspensions on glass substrates followed by heat-treatment at different temperatures. XRD was used to detect differences in the crystallinity between the reference TiO_2 sample treated at room temperature, 200 °C and 500 °C. From the XRD diffractograms (Figure 26), no discernable differences could be observed between the samples, which indicates that the sintering temperature does not significantly affect the crystallinity (or crystallite size) of the low-temperature processed TiO_2 photoanodes. This conclusion is also in good agreement with the study by Nakade et al.,[137] where no great difference in the XRD patterns could be seen when annealing TiO_2 films with similar compositions. In both studies, the TiO_2 anatase/rutile crystalline phase mass ratio was the same (about 85:15) as for the pristine P25 TiO_2 nanoparticles that were used as the main component in the paste. It is worth noting that the commercial P25 TiO_2 nanoparticles have already been heat treated at high temperatures during their production, meaning that the only major change during the subsequent heat treatments should be from the titanium isopropoxide used in the prepared suspensions. Furthermore, the addition of plasmonic particles to the TiO_2 paste did not significantly alter the XRD patterns, showing similar ratios as the pure TiO_2 reference samples.

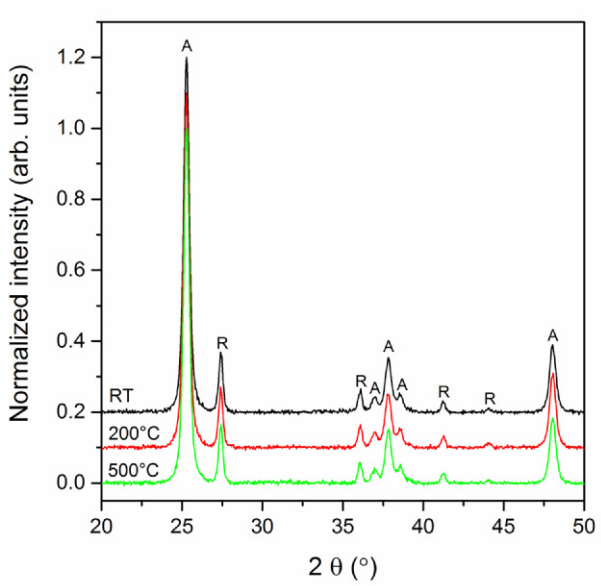

Figure 26. XRD plots of the TiO_2 reference sample treated at different temperatures. The letter "A" indicates reflections from the anatase crystal form, while "R" refers to rutile TiO_2. The diffractograms have been offset for clarity.

The optical properties of the composite TiO_2 films can be seen in Figure 27, where UV-vis transmission, reflectance and calculated absorptance spectra of TiO_2 films containing AuNRs are shown. When embedded in a TiO_2 matrix, the absorption of the particles will shift due to the change in the dielectric constant of the medium and due to the immobilization on the substrate. The AuNRs still exhibit their characteristic two absorption peaks (corresponding to the transverse (T) and longitudinal (L) peaks in Figure 27d). However, in comparison to the AuNR absorption spectra in solution, a clear shift towards lower wavelengths is evident. This is either due to small structural deformation of the particles or an effect from the TiO_2 matrix, as previously stated. The reflectance of the films remains mostly unchanged, indicating that the incorporation of the plasmonic materials mainly affects the light absorption properties of the TiO_2 films.

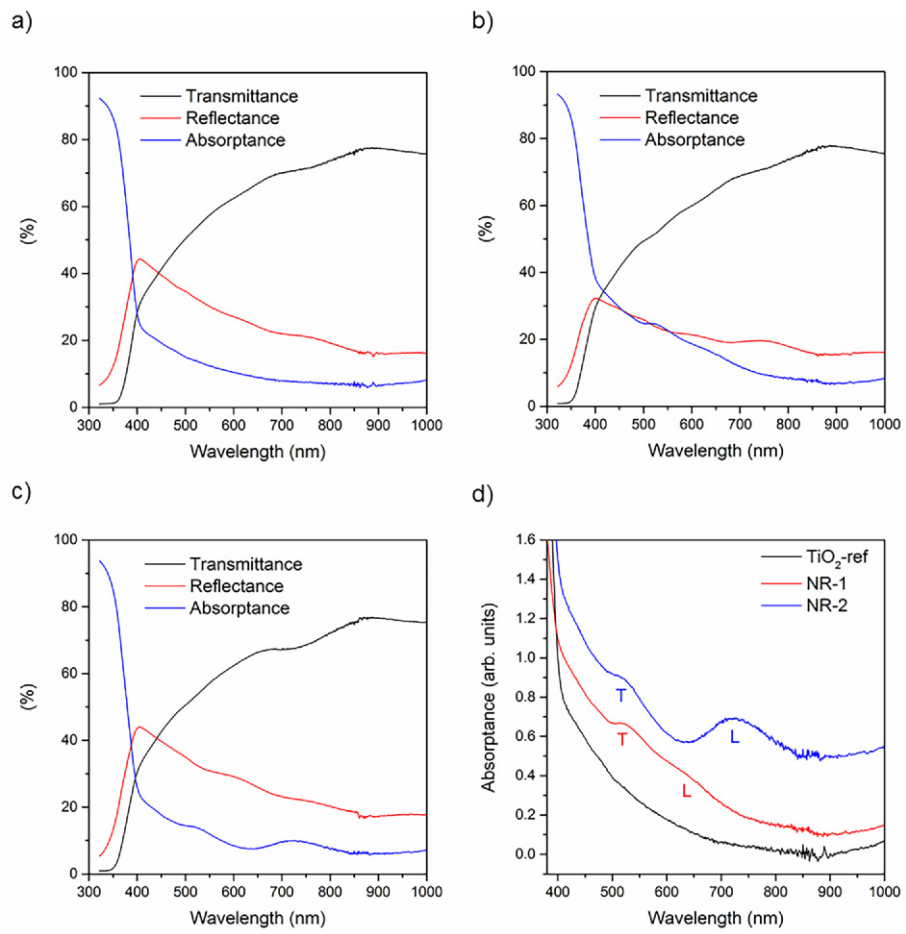

Figure 27. UV-vis spectra of transmittance, reflectance and absorptance of reference TiO_2 films (a) and TiO_2 films containing different aspect ratio AuNRs (a–c), and a absorptance spectra of all samples (d).

The structural details of the low-temperature processed films were studied in more detail using SEM. Figure 28 shows the top-view SEM images of the reference TiO_2 film and samples containing short aspect ratio nanorods (NR-1) and long aspect ratio nanorods (NR-2), respectively. Almost no noticeable differences can be seen between the samples, showing similar porous film structure without any larger cracks or aggregates. From the higher magnifications in the insets, it is possible to discern the size of the loosely aggregated particles (~13 ± 2 nm for all three samples). The particles were formed into an open porous network, where the TiO_2 originating from the titanium isopropoxide functioned as a binder.

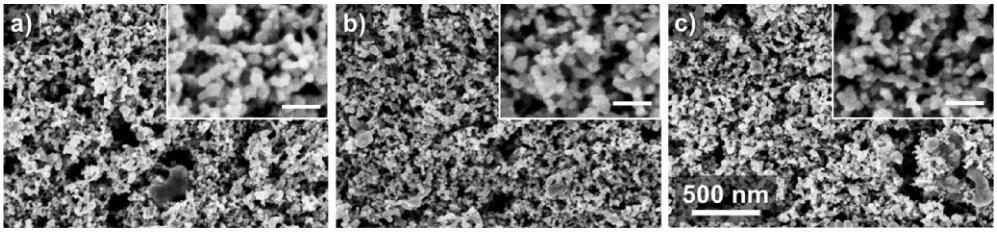

Figure 28. SEM images of the dip-coated films: a) TiO_2 reference, b) NR-1, and c) NR-2. Insets: Higher magnification of the structure showing the connectivity of the particles (scale bar: 50 nm).

Based on the SEM analysis, no discernable difference on the nanometer scale between the films was detected. To further compare the surface roughness and topography of the films, SWLI was used. From the SWLI images (Figure 29), larger variations in the surface structure can be seen between the samples compared to the SEM analysis. The reference TiO_2 sample appeared to have a more uniform structure than the films containing AuNRs (NR-1 and NR-2). These structural differences arise either from the titanium isopropoxide in the paste reacting with the trace amounts of reactants remaining from the core-shell nanoparticle synthesis, or from a detrimental effect of the added Au@SiO_2 NPs on the grain coalescence and diffusion process during the formation of the TiO_2 matrix.[138] This affects the particle binding and film formation, and could be a possible reason for the larger roughness of the plasmonic films.

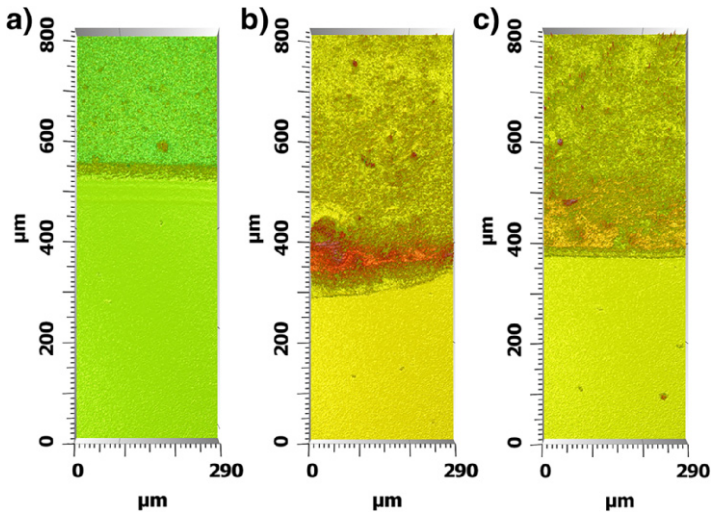

Figure 29. SWLI images of dip-coated films on glass slides: a) TiO_2 reference, b) NR-1, and c) NR-2. The smooth bottom parts depict the bare FTO substrate, while the thicker and coarser upper parts show the single layer dip-coated films.

5.3 Sensitized films

As mentioned in Section 2.3.1, the most commonly used sensitizers in DSSCs are ruthenium-complexes, due to their beneficial properties and high performance. In the DSSCs in Papers I and II, the ruthenium dye N719 was used, and the polymeric dye PT-C 85 was used in Paper III. The molecular structure of the sensitizers used in the studies were shown in Figure 15, while the UV-vis spectra of the sensitizers in solution are shown in Figure 30.

The use of polymeric sensitizers can be problematic due to the possible difficulty of penetration into the mesoporous network due to the size of the polymer. However, based on previous studies, the PT-C 85 polymer with a M_W between 1000–3000 penetrates easily into the pores and adsorbs onto the TiO_2 surface.[125]

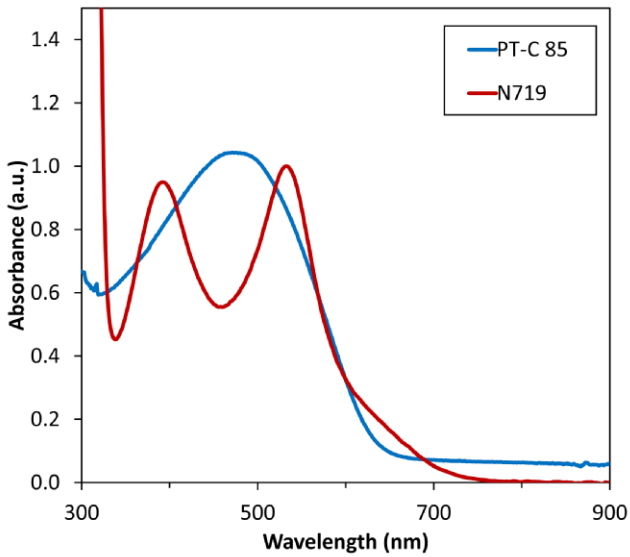

Figure 30. UV-vis spectra of the N719 dye and PT-C 85 sensitizers in solution.

When plasmonic particles are in close proximity of a sensitizer with suitable absorption, an enhancing effect can be seen. This is shown in Figure 31, where UV-vis spectra of PT-C 85 polymer solutions with different amounts of added core-shell plasmonic particles are shown. The absorption enhancement is calculated by subtracting the absorption spectra of the solutions without any added plasmonic particles from the spectra with added plasmonic particles. A clear increase in the absorption can be seen with increasing particle concentration, indicating an enhancing effect due to the presence of plasmonic particles. It is worth noting that the absorption spectrum will change when the sensitizer is adsorbed onto a substrate or porous scaffold due to the change of the dielectric constant of the surrounding medium.

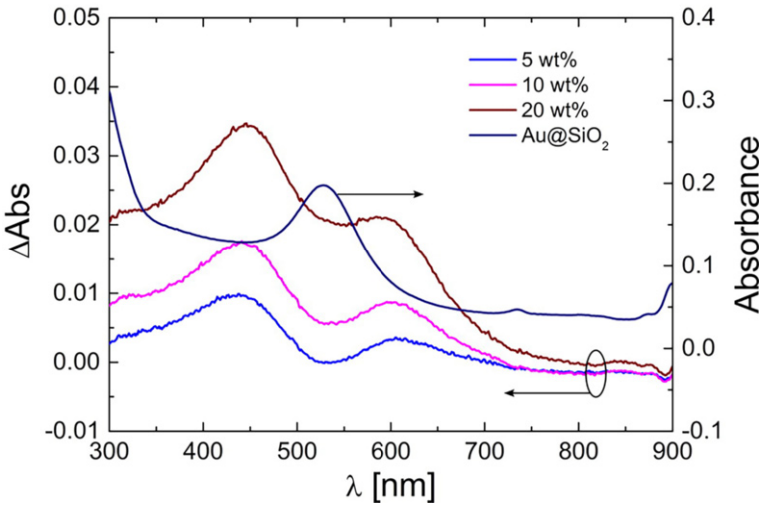

Figure 31. UV-vis spectra of the absorption enhancement caused by addition of increasing amounts of Au@SiO_2 NPs to PT-C 85 solutions.

5.3.1 Modeling

In order to further study the effect of the plasmonic enhancement of the Au@SiO_2 NPs on the sensitizers in the solar cells, the far-field and near-field properties of these particles were simulated. The scattering (far-field) coefficient (Q_{sca}) and near-field coefficient (Q_{NF}) for Au@SiO_2 NPs with a 16 nm gold core and 4 nm SiO_2 shell as a function of wavelength are shown in Figure 32a. The maximum of the near-field coefficient was slightly red-shifted and by three orders of magnitude higher compared to the maximum of the scattering coefficient. However, despite this large enhancement of the near-field, the enhancement can only affect the absorption when the absorbing dye is in close proximity to the plasmonic particle. The intensity enhancement of a core-shell particle was also modeled (Figure 32b). Light at 520 nm incident upon the particle along the z-axis excites the plasmon resonance, leading to increased fields near the surface of the particle. A strong enhancement was obtained within 5 nm from the outside of the SiO_2 shell, as seen by the red shaded half circle area in Figure 32b. These results indicate that for near-field enhancement of the absorption to occur, the plasmonic core-shell particles must be in close proximity to the absorbing sensitizer. Since the plasmonic core-shell particles used have been incorporated into the TiO_2 matrix, a majority should be located on the surface of the mesoporous TiO_2 film in the photoanode. Thus, the sensitizer adsorbed onto the TiO_2 is in close proximity to the Au@SiO_2 nanoparticles, enabling efficient near-field enhancement to take place.

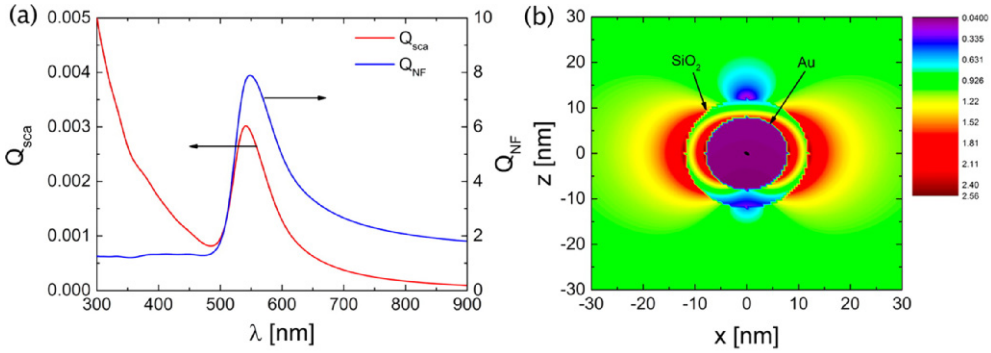

Figure 32. (a) The scattering constant Q_{sca} and the near-field constant Q_{NF} and (b) a 2D plot of the near-field intensity enhancement for an Au@SiO_2 particle with a 16 nm gold core and 4 nm SiO_2 shell at excitation at 520 nm.

5.4 Device performance

A summary of the solar cell performance for the champion cells used in the studies are given in Table 1.

In Paper I, the enhancing effect of plasmonic particles on DSSCs using N719 as sensitizer dye was investigated. The plasmonic particles coated with a thin SiO_2

Table 1. Summary of solar cell performance for champion cells in the studies.

	Plasmonic material	Sensitizer	Layer thickness (μm)	J_{SC} (mA/cm²)	V_{OC} (V)	*FF*	η (%)
Paper I	Au@SiO_2 nanoparticles	N719	1.90	3.90	0.85	0.68	2.30
	Reference	N719	1.87	3.40	0.85	0.69	2.00
Paper II	Au@SiO_2 nanorods (AR: 1.7)	N719	1.0 ± 0.2	1.1 ± 0.1	0.68 ± 0.02	0.68 ± 0.02	0.52 ± 0.06
	Au@SiO_2 nanorods (AR: 3.2)	N719	1.7 ± 0.2	1.8 ± 0.1	0.69 ± 0.01	0.73 ± 0.01	0.90 ± 0.04
	Reference	N719	1.6 ± 0.3	1.8 ± 0.4	0.68 ± 0.02	0.71 ± 0.03	0.88 ± 0.10
Paper III	Au@SiO_2 nanoparticles	PT-C-85	1.80	2.7 ± 0.08	0.56 ± 0.05	0.56 ± 0.01	0.87 ± 0.35
	Reference	PT-C-85	1.80	2.04 ± 1.4	0.52 ± 0.01	0.54 ± 0.04	0.58 ± 0.43
	Au@SiO_2 nanoparticles	PT-C-85	3.50	4.55 ± 0.08	0.54 ± 0.02	0.54 ± 0.01	1.32 ± 0.01
	Reference	PT-C-85	3.50	4.14 ± 0.06	0.51 ± 0.01	0.55 ± 0.01	1.2 ± 0.02
	Au@SiO_2 nanoparticles	PT-C-85	5.00	6.0 ± 0.1	0.53 ± 0.01	0.51 ± 0.01	1.62 ± 0.01
	Reference	PT-C-85	5.00	5.3 ± 0.4	0.50± 0.01	0.54 ± 0.01	1.42 ± 0.10

shell using the MPTMS method were stable against the liquid electrolyte, showing no dissolution after prolonged exposure. Many previous studies regarding the use of plasmonic particles in DSSCs have neglected to take into account the nanoparticle stability. Devices with and without added spherical $Au@SiO_2$ NPs were assembled and the PV properties were measured. The J-V curves and the IPCE spectra of the devices are shown in Figure 33. From the J-V plot (Figure 33a), a clear increase in the current density (J_{SC}) can be seen when comparing DSSCs with 1 wt% incorporated core-shell particles to the reference devices, resulting in an increase of the conversion efficiency from 2.00 to 2.30% (an increase by 15%). In the IPCE spectra (Figure 33b), an enhancement can be seen in the wavelength range of 500–550 nm in the devices with added plasmonic nanoparticles. This wavelength range corresponds to the surface plasmon wavelength of the nanoparticles, indicating that the particles enhance the light absorption of the dye.

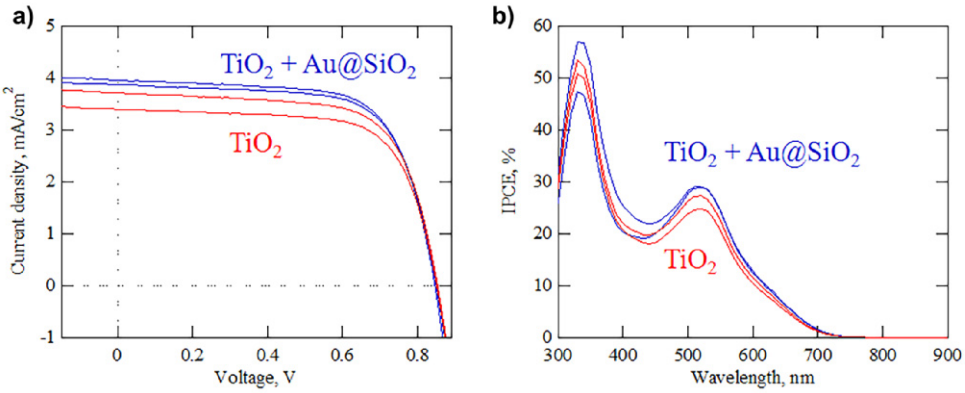

Figure 33. J-V curves (a) and IPCE spectra (b) of DSSCs with added core-shell particles.

In Paper II, the impact of anisotropic plasmonic nanoparticles on the PV properties of DSSCs was studied using the standard N719 dye as the sensitizer. Representative J-V curves are shown in Figure 34a. With efficiencies below 1% for all samples, the performance of these devices was poor compared to other DSSCs reported in the literature. This could be linked to the low film thickness, the high porosity of the films, and to the poor crystallinity of the TiO_2 portion produced from the titanium isopropoxide precursor. Furthermore, the results are in contrast with Paper I and previous studies,[108,109,118,119] where incorporation of plasmonic particles in the photoanode led to an enhancing effect. The main reason for the poor efficiencies is the low J_{SC} values. The reason for these low values is probably the detrimental effect that the plasmonic particles have on the structure of the photoanode, decreasing the amount of dye adsorbed to the surface and thus leading to a lower optical density of the samples. However, when examining the averaged IPCE spectra (Figure 34b), a clear increase and shift was seen at 550 nm and above for

the samples containing plasmonic particles. This would indicate a contribution from the plasmonic particles to the photon absorption in the device. When correcting for the lower dye amounts in the plasmonic devices, one would obtain higher J_{SC} and efficiency values than obtained for the reference devices.

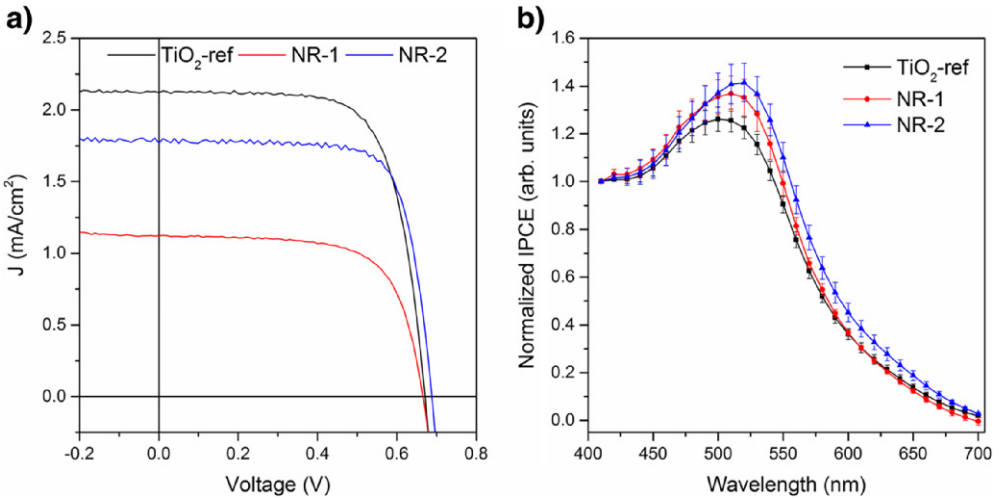

Figure 34. a) Representative J-V curves for the different samples, and b) averaged IPCE spectra, which have been normalized at 410 nm (n = 3–4).

In Paper III, plasmonic core-shell nanoparticles were added to a mesoporous TiO_2 layer sensitized with a polythiophene derivative PT-C 85, which was further assembled into solar cells. The PV properties of the devices were investigated, and the enhancing effects were related to a combination of near-field and far-field effects originating from the plasmonic particles.

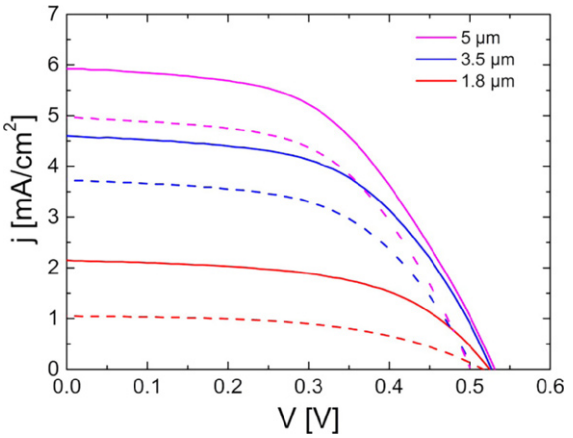

Figure 35. Representative J-V curves for plasmon (solid line) and TiO_2 reference (dashed) DSSC devices with varying photoanode layer thickness.

From the summary given in Table 1, it can be seen that the Jsc has increased in all the plasmon devices with a slight variation in the *FF*. A slight increase in the V_{OC} is also seen in all plasmonic devices. The highest enhancement in the performance is seen for the devices with thinnest (1.8 μm) TiO_2 layer, leading to a 67% increase in the efficiency. This enhancing effect is smaller for the devices with thicker TiO_2 layers; both 3.5 μm and 5 μm thick layers give ~13% efficiency increase. This overall increase in the efficiency is correlated with the improvements seen in the IPCE spectra (Figure 36a). A broad enhancement in the spectra can be seen for all devices containing plasmonic particles. In Figure 36b, the IPCE enhancement for the devices with 3.5 μm and 5 μm thick photoanodes is shown, and the 1.8 μm thick device is shown in the inset. The IPCE enhancement was calculated by subtracting the reference IPCE spectra from the plasmonic sample IPCE spectra. The largest enhancement can be seen around 560 nm, which is close to the LSPR wavelength of the plasmonic nanoparticles.

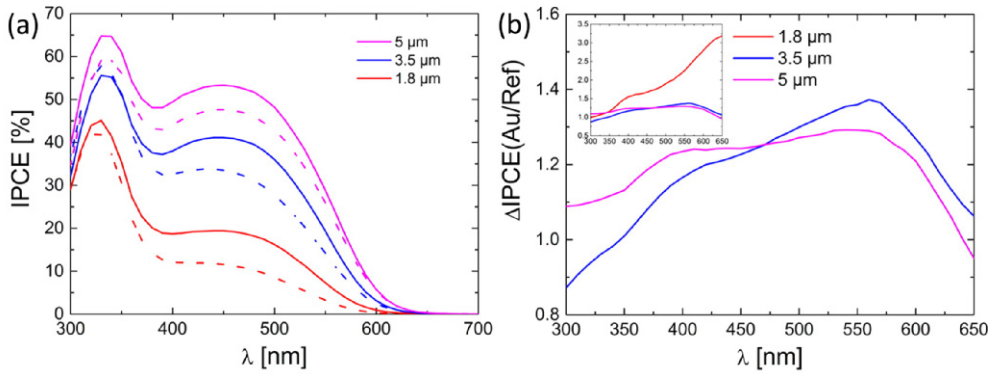

Figure 36. (a) Representative IPCE spectra for the plasmon (solid) and TiO_2 reference (dashed) DSSC devices at different thicknesses and (b) the IPCE enhancement for the 3.5 μm and 5 μm thick devices showing a maximum enhancement at 560 nm. The enhancement including the 1.8 μm device is shown in the inset.

6 Conclusions

The overall aim of this thesis was to design plasmonic materials suitable for incorporation in dye-sensitized solar cells (DSSCs) and polymer-sensitized solar cells (PSSCs) and to investigate the effects of the added materials on the device performance. The presented studies have shown that several crucial factors need to be considered when incorporating plasmonic materials in these devices. Firstly, the materials need to withstand the processing conditions and the environment in the cells without deformation or dissolution. Secondly, the materials should have minimal negative effect on the device performance, i.e. not change the structure of the semiconductor layer or affect the charge mobility or quenching of the charge carriers. Finally, the optical properties of the materials need to be closely matched to that of the sensitizer used in the devices for efficient enhancement. In practice, this means that the absorption wavelength of the plasmonic nanoparticles should be close to the absorption of the dye/polymer sensitizer used in the DSSCs/PSSCs.

It has been shown that gold nanoparticles can be synthesized in a wide variety of sizes and shapes and be coated with a thin silica shell using a variety of methods. The coating methods, although simple, are very sensitive to both synthesis conditions and compound purity. In the studies, when synthesizing the silica shell, the method using (3-mercaptopropyl)trimethoxysilane (MPTMS) as a linking molecule gave the best results. Thin (~5 nm) silica shells were formed around the gold cores, which enabled the particles to be used together with the aggressive liquid iodine/triiodide electrolyte while still maintaining their optical characteristics. Furthermore, these core-shell particles could withstand the heating process during photoanode preparation without deforming or cracking the shell. This enabled the spherical particles to be used in combination with current processing techniques for DSSCs.

However, spectrometry and transmission electron microscopy (TEM) studies showed that gold nanorods are thermally stable only up to 200 °C. TiO_2 suspensions suitable for low-temperature processing were developed and utilized to prepare mesoporous TiO_2 films containing core-shell gold nanorods (Au@SiO_2 NRs). By using a range of structural characterization techniques, it was possible to determine how the addition of the Au@SiO_2 NRs affected the structure of the produced films as well as show minimal deformation of the gold nanorods after photoanode processing. This is a crucial factor, since several previous studies have failed to take the effect of the processing temperature into account when utilizing anisotropic particles.

The DSSC devices with incorporated spherical core-shell gold nanoparticles (Au@SiO_2 NPs) showed an enhancement in the incident photon to electron conversion efficiency (IPCE) spectrum corresponding to the plasmon wavelength at around 550 nm. This enhancement resulted in a ~10% improvement of the overall efficiency. The devices with added Au@SiO_2 NRs revealed a clear red shift

of the peak in the IPCE spectra in the 500–520 nm range and, after normalizing the spectra, an enhancement in the 500–700 nm wavelength range. Thus, the minimal structural deformation of the gold nanorods, when using the low-temperature processing method, allowed to demonstrate the potential of using $Au@SiO_2$ NRs to enhance the performance in the sub-near-infrared (NIR) wavelength range.

Finally, $Au@SiO_2$ NPs were utilized in PSSCs using a copolymer as a sensitizer. Different photoanode thicknesses were evaluated, with the largest relative increase from the thinnest one. An improved performance due to increased short-circuit current could be seen for all device thicknesses with added plasmonic particles. The amplified current was attributed to an increase in the photon absorption as observed from the IPCE spectra. Additionally, the near-field and far-field effects of the $Au@SiO_2$ NPs were modeled, showing that the enhancement is due a combination of near-field (absorption) and far-field (scattering) effects leading to an increased photon absorption close to the particle surface.

The results presented in this thesis show that the use of plasmonic materials can have a significant impact on the optical properties and performance of solar cells. However, in order to fully utilize these materials, careful control over the synthesis and processing conditions of the materials is needed to obtain materials with the desired size and shape that are also chemically and thermally stable in the required applications. Furthermore, control over the processing conditions and an understanding of how these factors can influence the physical properties of nanoparticles is crucial for effective and reproducible application of plasmonic materials.

As indicated in the studies, the effect of plasmonic particles is more prominent when integrated into thin (~2 μm) semiconductor films. This would make the utilization of plasmonic particles suitable for applications where device thickness is a limiting factor, such as in integrated devices to power sensors or other electronics. Additionally, compared to other photon management strategies, such as the use of light scattering particles and structures, the use of plasmonic particles offer the possibility to tailor the optical response to match the sensitizer. Although these studies have been limited to utilizing gold nanoparticles with optical responses in the visible region, other materials, such as metal chalcogenides or metal oxides, give the possibility to extend the optical response into the NIR region. Another possible approach to extend the optical response would be to adjust the shape of the plasmonic materials to make more exotic structures, such as branched networks, ordered arrays of particles, etc. By understanding the properties and limitations of the used materials and carefully controlling the size and shape of the synthesized particles, the use of plasmonic materials gives a large library of materials and particle shapes making it possible to tailor the optical response from ultraviolet to NIR light.

7 References

[1] Feldman D., Barbose G., Margolis R., Bolinger M., Chung D., Fu R., Seel J., Davidson C., Darghouth N. and Wiser R., Photovoltaic System Pricing Trends: Historical, Recent, and Near-Term Projections 2015 Edition, National Renewable Energy Laboratory (2016) (available from: https://dx.doi.org/10.7799/1254998)

[2] Parida B., Iniyan S. and Goic R., A review of solar photovoltaic technologies, Renewable and Sustainable Energy Reviews, 15, 1625–1636 (2011)

[3] Conibeer G. and Willoughby A., Solar Cell Materials: Developing Technologies. John Wiley & Sons, Ltd, Chichester, UK (2014)

[4] Krč J., Lipovšek B. and Topič M., Light Management in Thin-Film Solar Cell. In: Cristóbal López A., Martí Vega A. and Luque López A. (eds), Next Generation of Photovoltaics, Springer Series in Optical Sciences, vol 165. Springer, Berlin, Heidelberg (2012)

[5] Jimenez de Aberasturi D., Serrano-Montes A.B. and Liz-Marzán L.M., Modern Applications of Plasmonic Nanoparticles: From Energy to Health, Advanced Optical Materials, 3, 602–617 (2015)

[6] Fröhlich, C. and Lean, J., Solar radiative output and its variability: evidence and mechanisms, The Astronomy and Astrophysics Review, 12, 273–320 (2004)

[7] Solar spectrum (available from: https://en.wikipedia.org/wiki/File:Solar_spectrum_en.svg)

8 Schmalensee R., Bulovic V., Armstrong R., Batlle C., Brown P., Deutch J., Jacoby H., Jaffe R., Jean J., Miller R., O'Sullivan F., Parsons J., Pérez-Arriaga J.I., Seifkar N., Stoner R. and Vergara C., The Future of Solar Energy: An Interdisciplinary MIT Study. Massachusetts Institute of Technology, MIT Energy Initiative (2015) (available from: http://mitei.mit.edu/futureofsolar)

[9] Kirchartz T., Bisquert J., Mora-Sero I. and Garcia-Belmonte G., Classification of solar cells according to mechanisms of charge separation and charge collection, Physical Chemistry Chemical Physics, 17, 4007–4014 (2017)

[10] Jean J., Brown P.R., Jaffe R.L., Buonassisi T. and Bulović V., Pathways for solar photovoltaics, Energy and Environmental Science, 8, 1200–1219 (2015)

[11] Asim N., Sopian K., Ahmadi S., Saeedfar K., Alghoul M.A., Saadatian O. and Zaidi S.H., A review on the role of materials science in solar cells, Renewable and Sustainable Energy Reviews, 16, 5834–5847 (2012)

[12] Philipps S. and Warmuth W., Fraunhofer ISE: Photovoltaics Report (2017) (available from: https://www.ise.fraunhofer.de/de/veroeffentlichungen/studien/photovoltaics-report.html)

[13] Vegad M. and Bhatt N.M., Review of some Aspects of Single Crystal Growth Using Czochralski Crystal Growth Technique, Procedia Technology, 14, 438–446 (2014)

[14] Föll H., Semiconductor Technology. University of Kiel (2014) (available from: https://www.tf.uni-kiel.de/matwis/amat/semitech_en/)

[15] Card H.C. and Yang E.S., Electronic processes at grain boundaries in polycrystalline semiconductors under optical illumination, IEEE Transactions on Electron Devices, ED-24, 397–402 (1977)

[16] Goldstein M., 450 mm silicon wafers challenges – wafer thickness scaling, ECS Transactions, 16, 3–13 (2008)

[17] Goodrich A., Hacke P., Wang Q., Sopori B., Margolis R., James T.L. and Woodhouse M., A wafer-based monocrystalline silicon photovoltaics road map: Utilizing known technology improvement opportunities for further reductions in manufacturing costs, Solar Energy Materials and Solar Cells, 114, 110–135 (2013)

[18] Moon S., Kim K., Kim Y., Heo J. and Lee J., Highly efficient single-junction GaAs thin-film solar cell on flexible substrate, Scientific Reports 6, 30107 (2016)

[19] Bauhuis G.J., Mulder P., Haverkamp E.J., Huijben J.C.C.M. and Schermer J.J., 26.1% thin-film GaAs solar cell using epitaxial lift-off, Solar Energy Materials and Solar Cells, 93, 1488–1491 (2009)

[20] Green M.A., Emery K., Hishikawa Y., Warta W., Dunlop E.D., Levi D.H. and Ho-Baillie A.W.Y., Solar cell efficiency tables (version 49), Progress in Photovoltaics: Research and Applications, 25, 3–13 (2017)

[21] Miles R.W., Photovoltaic solar cells: Choice of materials and production methods, Vacuum, 80, 1090–1097 (2006)

[22] Yamaguchi M., Takamoto T., Araki K. and Ekins-Daukes N., Multi-junction III–V solar cells: current status and future potential, Solar Energy, 79, 78–85 (2005)

[23] Olson J.M., Friedman D.J. and Kurtz S., High-Efficiency III-V Multijunction Solar Cells. In: Luque A. and Hegedus S. (eds), Handbook of Photovoltaic Science and Engineering. John Wiley & Sons, Ltd, Chichester, UK (2003)

[24] Carlson D.E. and Wronski C.R., Amorphous silicon solar cell, Applied Physics Letters, 28, 671 (1976)

[25] Shah A.V., Schade H., Vanecek M., Meier J., Vallat-Sauvain E., Wyrsch N., Kroll U., Droz C. and Bailat J., Thin-film silicon solar cell technology, Progress in Photovoltaics: Research and Applications, 12, 113–142 (2004)

[26] Crandall R.S., Defect relaxation in amorphous silicon: Stretched exponentials, the Meyer-Neldel rule, and the Staebler-Wronski effect, Physical Review B, 43, 4057–4070 (1991)

[27] McCandless B. E. and Sites J.R., Cadmium Telluride Solar Cells. In: Luque A. and Hegedus S. (eds), Handbook of Photovoltaic Science and Engineering, 2nd ed. John Wiley & Sons, Ltd, Chichester, UK (2010)

[28] Martin R., First Solar's Cells Break Efficiency Record, MIT Technology Review (2016) (available from: https://www.technologyreview.com/s/600922/first-solars-cells-break-efficiency-record/)

[29] Green M.A., Thin-film solar cells: review of materials, technologies and commercial status, Journal of Materials Science: Materials in Electronics, 18, 15–19 (2007)

[30] Romeo A., Terheggen M., Abou-Ras D., Bätzner D.L., Haug F.-J., Kälin M., Rudmann D. and Tiwari A.N., Development of thin-film Cu(In,Ga)Se_2 and CdTe solar cells, Progress in Photovoltaics: Research and Applications, 12, 93–111 (2004)

[31] DSSC image (available from: http://www.actu.epfl.ch)

[32] OPV image (available from: http://www.infinitypv.com)

[33] Shin B., Gunawan O., Zhu Y., Bojarczuk N.A., Chey S.J. and Guha S., Thin film solar cell with 8.4% power conversion efficiency using an earth-abundant Cu_2ZnSnS_4 absorber, Progress in Photovoltaics: Research and Applications, 21, 72–76 (2013)

[34] Todorov T.K., Reuter K.B. and Mitzi D.B., High-Efficiency Solar Cell with Earth-Abundant Liquid-Processed Absorber, Advanced Materials, 22, E156–E159 (2010)

[35] Kippelen B. and Brédas J.-L., Organic Photovoltaics, Energy & Environmental Science, 2, 251–261 (2009)

[36] Brabec C., Dyakonov V. and Scherf U., Organic Photovoltaics: Materials, Device Physics, and Manufacturing Technologies. Wiley-VCH Verlag GmbH & Co. KGaA, Weinheim (2008)

[37] Zhan X. and Zhu D., Conjugated polymers for high-efficiency organic photovoltaics, Polymer Chemistry, 1, 409–419 (2010)

[38] Zhou Y., Fuentes-Hernandez C., Khan T.M., Liu J.-C., Hsu J., Shim J.W., Dindar A., Youngblood J.P., Moon R.J. and Kippelen B., Recyclable organic solar cells on cellulose nanocrystal substrates, Scientific Reports, 3, 1536 (2013)

[39] Carey G.H., Abdelhady A.L., Ning Z., Thon S.M., Bakr O.M. and Sargent, E.H., Colloidal Quantum Dot Solar Cells, Chemical Reviews, 115, 12732–12763 (2015)

[40] Kamat P.V., Quantum Dot Solar Cells. Semiconductor Nanocrystals as Light Harvesters, The Journal of Physical Chemistry C, 112, 18737–18753 (2008)

[41] Duan J., Zhang H., Tang Q., He B. and Yu L., Recent advances of critical materials in quantum dot–sensitized solar cells: a review, Journal of Materials Chemistry A, 3, 17497–17510 (2015)

[42] Hardin B.E., Snaith H.J. and McGehee M.D., The renaissance of dye-sensitized solar cells, Nature Photonics, 6, 162–169 (2012)

[43] Sugathan V., John E. and Sudhakar K., Recent improvements in dye sensitized solar cells: A review, Renewable and Sustainable Energy Reviews, 52, 54–64 (2015)

[44] Hagfeldt, A., Boschloo, G., Sun, L., Kloo, L. and Pettersson, H., Dye-Sensitized Solar Cells, Chemical Reviews, 110, 6595–6663 (2010)

[45] Yang L., Barrows A.T., Lidzey D.G. and Wang T., Recent progress and challenges of organometal halide perovskite solar cells, Reports on Progress in Physics, 79, 026501 (2016)

[46] Jeon N.J., Noh J.H., Yang W.S., Kim Y.C., Ryu S., Seo J. and Seok S.I., Compositional engineering of perovskite materials for high-performance solar cells, Nature, 517, 476–480 (2015)

[47] Niu G., Guo X. and Wang L., Review of recent progress in chemical stability of perovskite solar cells, Journal of Materials Chemistry A, 3, 8970–8980 (2015)

[48] Ye M., Hong X., Zhang F. and Liu X., Recent Advancements in Perovskite Solar Cells: Flexibility, Stability and Large Scale, Journal of Materials Chemistry A, 4, 6755–6771(2016)

[49] Grätzel, M., Mesoscopic Solar Cells, 79–96. In: Richter C., Lincot D. and Gueymard C.A. (eds), Solar Energy. Springer, New York (2013)

[50] Rhee J.H., Chung C.-C. and Diau E.W.-G., A perspective of mesoscopic solar cells based on metal chalcogenide quantum dots and organometal-halide perovskites, NPG Asia Materials, 5, e68 (2013)

[51] Grätzel M., Recent Advances in Sensitized Mesoscopic Solar Cells, Accounts of Chemical Research, 42, 1788–1798 (2009)

[52] Tributsch H., Reaction of Excited Chlorophyll Molecules at Electrodes and in Photosynthesis, Photochemistry and Photobiology, 16, 261–269 (1972)

[53] Tsubomura H., Matsumura M., Nomura Y. and Amamya T., Dye sensitised zinc oxide: aqueous electrolyte: platinum photocell, Nature, 261, 402–403 (1976)

[54] O'Regan B. and Grätzel M., A low-cost, high-efficiency solar cell based on dye-sensitized colloidal TiO_2 films, Nature, 353, 737–740 (1991)

[55] NREL: National Center for Photovoltaics, Research Cell Efficiency Records (available from: https://www.nrel.gov/pv/assets/images/efficiency-chart.png)

[56] Parisi M.L., Maranghi S. and Basosi R., The evolution of the dye sensitized solar cells from Grätzel prototype to up-scaled solar applications: a life cycle assessment approach, Renewable & Sustainable Energy Reviews, 39, 124–138 (2014)

[57] Freitag M., Teuscher J., Saygili Y., Zhang X., Giordano F., Liska P., Hua J., Zakeeruddin S.M., Moser J.-E., Grätzel M. and Hagfeldt A., Dye-sensitized solar cells for efficient power generation under ambient lighting, Nature Photonics, 11, 372–378 (2017)

[58] Asghar M.I., Stability issues of dye solar cells, Aalto University publication series Doctoral Dissertations, 53/2012 (2012)

[59] Ye M., Wen X., Wang M., Iocozzia J., Zhang N., Lin C. and Lin Z., Recent advances in dye-sensitized solar cells: from photoanodes, sensitizers and electrolytes to counter electrodes, Materials Today, 18, 155–162 (2015)

[60] Toivola M., Dye-sensitized solar cells on alternative substrates, TKK dissertations, 214 (2010)

[61] Yeoh M.-E., and Chan K.-Y., Recent advances in photo-anode for dye-sensitized solar cells: a review, International Journal of Energy Research, 41, 2446–2467 (2017)

[62] Yandong D., Nianqing F., Qiuping L., Yanyan F., Xiaowen Z., Jingbo Z. and Yuan L., Sn-Doped TiO_2 Photoanode for Dye-Sensitized Solar Cells, The Journal of Physical Chemistry C, 116, 8888–8893 (2012)

[63] Fan K., Yu J. and Ho W., Improving photoanodes to obtain highly efficient dye-sensitized solar cells: a brief review, Materials Horizons, 4, 319–344 (2017)

[64] Goldschmidt J.C. and Fischer S., Upconversion for Photovoltaics – a Review of Materials, Devices and Concepts for Performance Enhancement, Advanced Optical Materials 3, 510–535 (2015)

[65] Hwang H.-J., Joo S.-J., Patil S.A. and Kim H.-S., Efficiency enhancement in dye-sensitized solar cells using the shape/size-dependent plasmonic nanocomposite photoanodes incorporating silver nanoplates, Nanoscale, 9, 7960–7969 (2017)

[66] Shalini S., Balasundaraprabhu R., Kumar T.S., Prabavathy N., Senthilarasu S. and Prasanna S., Status and outlook of sensitizers/dyes used in dye sensitized solar cells (DSSC): a review, International Journal of Energy Research, 40, 1303–1320 (2016)

[67] Lee C.-P., Lin R.Y.-Y., Lin L.-Y., Li C.-T., Chu T.-C., Sun S.-S., Lin J.T. and Ho K.-C., Recent progress in organic sensitizers for dye-sensitized solar cells, RSC Advances, 5, 23810–23825 (2015)

[68] Wu J., Lan Z., Lin J., Huang M., Huang Y., Fan L. and Luo G., Electrolytes in Dye-Sensitized Solar Cells, Chemical Reviews, 115, 2136–2173 (2015)

[69] Gorlov M. and Kloo L., Ionic liquid electrolytes for dye-sensitized solar cells, Dalton Transactions, 20, 2655–2666 (2008)

[70] Zhang J., Freitag M., Hagfeldt A. and Boschloo G., Solid-State Dye-Sensitized Solar Cells. In: Tian H., Boschloo G. and Hagfeldt A. (eds), Molecular Devices for Solar Energy Conversion and Storage, Green Chemistry and Sustainable Technology. Springer, Singapore (2018)

[71] Thomas S., Deepak T.G., Anjusree G.S., Arun T.A., Nair S.V. and Nair A.S., A review on counter electrode materials in dye-sensitized solar cells, Journal of Materials Chemistry A, 2, 4474–4490 (2014)

[72] Ye M., Wen X., Wang M., Iocozzia J., Zhang N., Lin C. and Lin Z., Recent advances in dye-sensitized solar cells: from photoanodes, sensitizers and electrolytes to counter electrodes, Materials Today, 18,155–162 (2015)

[73] Hara K. and Koumura N., Organic Dyes for Efficient and Stable Dye-Sensitized Solar Cells, Material Matters, 4.4, 92 (2009)

[74] Wu M. and Ma T., Recent Progress of Counter Electrode Catalysts in Dye-Sensitized Solar Cells Journal of Physical Chemistry C, 118, 16727–16742 (2014)

[75] Barnes W.L., Dereux A. and Ebbesen T.W., Surface plasmon subwavelength optics, Nature, 424, 824–830 (2003)

[76] Zayats A.V. and Smolyaninov I.I., Near-field photonics: surface plasmon polaritons and localized surface plasmons, Journal of Optics A: Pure and Applied Optics, 5, S16 (2003)

[77] Schuller J.A., Barnar E.S., Cai W., Chul Jun Y., White J.S. and Brongersma M.L., Plasmonics for extreme light concentration and manipulation, Nature Materials, 9, 193–204 (2010)

[78] Schwartzberg A.M., Grant C.D., Wolcott A., Talley C.E., Huser T.R., Bogomolni R. and Zhang J.Z., Unique Gold Nanoparticle Aggregates as a Highly Active Surface-Enhanced Raman Scattering Substrate, Journal of Physical Chemistry B, 108, 19191–19197 (2004)

[79] Saha K., Agasti S.S., Kim C., Li X. and Rotello V.M., Gold Nanoparticles in Chemical and Biological Sensing, Chemical Reviews, 112, 2739–2779 (2012)

[80] Dreaden E.C., Alkilany A.M., Huang X., Murphy C.J. and El-Sayed M.A., The golden age: gold nanoparticles for biomedicine, Chemical Society Reviews, 41, 2740–2779 (2012)

[81] Erwin W.R., Zarick H.F., Talbert E.M. and Bardhan R., Light trapping in mesoporous solar cells with plasmonic nanostructures, Energy & Environmental Science, 9, 1577–1601 (2016)

[82] Catchpole K.R. and Polman A., Plasmonic solar cells, Optics Express, 16, 21793 (2008)

[83] Atwater H.A. and Polman A., Plasmonics for improved photovoltaic devices, Nature Materials, 9, 205–213 (2010)

[84] Jiang R., Li B., Fang C. and Wang J., Metal/Semiconductor Hybrid Nanostructures for Plasmon-Enhanced Applications, Advanced Materials, 26, 5274–5309 (2014)

[85] Louis C. and Pluchery O., Gold Nanoparticles for Physics, Chemistry and Biology, Imperial College Press, London (2012)

[86] Pelton M. and Bryant G.W., Introduction to Metal-Nanoparticle Plasmonics. John Wiley & Sons, Ltd, ProQuest Ebook Central (2013)

[87] Motl N.E., Smith A.F., DeSantis C.J. and Skrabalak S.E., Engineering plasmonic metal colloids through composition and structural design, Chemical Society Reviews, 43, 3823–3834 (2014)

[88] Rao C.N.R., Kulkarni G.U., Thomas P.J. and Edwards P.P., Metal nanoparticles and their assemblies, Chemical Society Reviews, 29, 27–35 (2000)

[89] Roduner E., Size matters: why nanomaterials are different, Chemical Society Reviews, 35, 583–592 (2006)

[90] Daniel M.-C. and Astruc D., Gold Nanoparticles: Assembly, Supramolecular Chemistry, Quantum-Size-Related Properties, and Applications toward Biology, Catalysis, and Nanotechnology, Chemical Reviews, 104, 293–346 (2004)

[91] Xia Y., Xiong Y., Lim B. and Skrabalak S.E., Shape-Controlled Synthesis of Metal Nanocrystals: Simple Chemistry Meets Complex Physics?, Angewandte Chemie International Edition, 48, 60–103 (2008)

[92] Ni W., Kou X., Yang Z. and Wang J., Tailoring Longitudinal Surface Plasmon Wavelengths, Scattering and Absorption Cross Sections of Gold Nanorods, ACS Nano, 2, 677–686 (2008)

[93] Murphy C.J., Sau T.K., Gole A.M., Orendorff C.J., Gao J., Gou L., Hunyadi S.E. and Li T., Anisotropic Metal Nanoparticles: Synthesis, Assembly, and Optical Applications, The Journal of Physical Chemistry B, 109, 13857–13870 (2005)

[94] Chanana M. and Liz-Marzán L.M., Coating matters: the influence of coating materials on the optical properties of gold nanoparticles, Nanophotonics, 1, 199–220 (2012)

[95] Guerrero-Martínez A., Pérez-Juste J. and Liz-Marzán L.M., Recent Progress on Silica Coating of Nanoparticles and Related Nanomaterials, Advanced Materials, 22, 1182–1195 (2010).

[96] Iler R.K., The Chemistry of Silica: Solubility, Polymerization, Colloid and Surface Properties and Biochemistry of Silica, Wiley (1979)

[97] Guglielmi M., Sol-gel coatings on metals, Journal of Sol-Gel Science and Technology, 8, 443–449 (1997)

[98] Mann S., Burkett S.L., Davis S.A., Fowler C.E., Mendelson N.H., Sims S.D., Walsh D. and Whilton N.T., Sol–Gel Synthesis of Organized Matter, Chemistry of Materials, 9, 2300–2310 (1997)

[99] Park S.K., Kim K.D. and Kim H.T., Preparation of silica nanoparticles: determination of the optimal synthesis conditions for small and uniform particles, Colloids and Surfaces A: Physicochemical and Engineering Aspects, 197, 7–17 (2002)

[100] Graf C., Vossen D.L.J., Imhof A. and van Blaaderen A., A General Method to Coat Colloidal Particles with Silica, Langmuir, 19, 6693–6700 (2003)

[101] Stöber W., Fink A. and Bohn E., Controlled growth of monodisperse silica spheres in the micron size range, Journal of Colloid and Interface Science, 26, 62–69 (1968)

[102] Liu S. and Han M.-Y., Silica-Coated Metal Nanoparticles, Chemistry – An Asian Journal, 5, 36–45 (2010)

[103] Liz-Marzán L.M., Giersig M. and Mulvaney P., Synthesis of Nanosized Gold–Silica Core–Shell Particles, Langmuir, 12, 4329–4335 (1996)

[104] Sendroiu I.E., Warner M.E. and Corn R.M., Fabrication of Silica-Coated Gold Nanorods Functionalized with DNA for Enhanced Surface Plasmon Resonance Imaging Biosensing Applications, Langmuir, 25, 11282–11284 (2009)

[105] Chen M.M.Y. and Katz A., Synthesis and Characterization of Gold–Silica Nanoparticles Incorporating a Mercaptosilane Core-Shell Interface, Langmuir, 18, 8566–8572 (2002)

[106] Gangadharan D.T., Xu Z., Liu Y., Izquierdo R. and Ma D., Recent advancements in plasmon-enhanced promising third-generation solar cells, Nanophotonics, 6, 153–175 (2017)

[107] Pillai S. and Green M.A., Plasmonics for photovoltaic applications, Solar Energy Materials and Solar Cells, 94, 1481–1486 (2010)

[108] Brown, M.D., Suteewong T., Kumar R.S.S.K., D'Innocenzo V., Petrozza A., Lee M.M., Wiesner U. and Snaith H.J., Plasmonic Dye-Sensitized Solar Cells Using Core–Shell Metal–Insulator Nanoparticles, Nano Letters, 11, 438–445 (2011)

[109] Wang J., Lee Y.-J., Chadha A.S., Yi J., Jespersen M.L., Kelley J.J., Nguyen H.M., Nimmo M., Malko A.V., Vaia R.A., Zhou W. and Hsu J.W.P., Effect of Plasmonic Au Nanoparticles on Inverted Organic Solar Cell Performance, Journal of Physical Chemistry C, 117, 85–97 (2012)

[110] Carretero-Palacios S., Calco M.E. and Miguez H., Absorption Enhancement in Organic–Inorganic Halide Perovskite Films with Embedded Plasmonic Gold Nanoparticles, Journal of Physical Chemistry C, 119, 18635–18640 (2015)

[111] Jang Y.H., Jang Y.J., Kim S., Quan L.N., Chung K., and Kim D.H., Plasmonic Solar Cells: From Rational Design to Mechanism Overview, Chemical Reviews, 116, 14982-15034 (2016)

[112] Lim S.P., Pandikumar A., Huang N.M. and Lim H.N., Enhanced Photovoltaic Performance of Silver@Titania Plasmonic Photoanode in Dye-sensitized Solar Cells, RSC Advances, 4, 38111–38118 (2014)

[113] Huang P.-C., Chen T.-Y., Wang Y.-L., Wu C.-Y. and Lin T.-L., Improving Interfacial Electron Transfer and Light Harvesting in Dyesensitized Solar Cells by Using Ag Nanowire/TiO_2 Nanoparticle Composite Films, RSC Advances, 5, 70172–70177 (2015)

[114] Jang Y.H., Jang Y.J., Kochuveedu S.T., Byun M., Lin Z. and Kim D.H., Plasmonic Dye-Sensitized Solar Cells Incorporated with Au–TiO_2 Nanostructures with Tailored Configurations, Nanoscale, 6, 1823–1832 (2014)

[115] Sahu G., Gordon S.W. and Tarr M.A., Synthesis and Application of Core-Shell Au–TiO_2 Nanowire Photoanode Materials for Dye Sensitized Solar Cells, RSC Advances, 2, 573–582 (2012)

[116] Ding Y., Sheng J., Yang Z., Jiang L., Mo L. e., Hu L., Que Y. and Dai S., High Performance Dye-Sensitized Solar Cells with Enhanced Light-Harvesting Efficiency Based on Polyvinylpyrrolidone-Coated Au–TiO_2 Microspheres, ChemSusChem 9, 720–727 (2016)

[117] Liu B.-J., Lin K.-Q., Hu S., Wang X., Lei Z.-C., Lin H.-X. and Ren B., Extraction of Absorption and Scattering Contribution of Metallic Nanoparticles Toward Rational Synthesis and Application, Analytical Chemistry, 87, 1058–1065 (2015)

[118] Bai L., Li M., Guo K., Luoshan M., Mehnane H.F., Pei L., Pan M., Liao L. and Zhao X., Plasmonic enhancement of the performance of dye-sensitized solar cell by core–shell AuNRs@SiO_2 in composite photoanode, Journal of Power Sources, 272, 1100–1105 (2014)

[119] Chang S., Li Q., Xiao X., Wong K.Y. and Chen T., Enhancement of low energy sunlight harvesting in dye-sensitized solar cells using plasmonic gold nanorods, Energy & Environmental Science, 5, 9444–9448 (2012)

[120] Turkevich J., Garton G. and Stevenson P.C., The color of colloidal gold, Journal of Colloid Science, 9, 26–35 (1954)

[121] Nikoobakht B. and El-Sayed M.A., Preparation and Growth Mechanism of Gold Nanorods (NRs) Using Seed-Mediated Growth Method, Chemistry of Materials, 15, 1957–1962 (2003)

[122] Ito S., Chen P., Comte P., Nazeeruddin M.K., Liska P., Pechy P. and Grätzel M., Fabrication of screen-printing pastes from TiO_2 powders for dye-sensitised solar cells, Progress in Photovoltaics: Research and Applications, 15, 603–612 (2007)

[123] Zhang D., Yoshida T., Oekermann T. and Furuta K., Room-Temperature Synthesis of Porous Nanoparticulate TiO_2 Films for Flexible Dye-Sensitized Solar Cells, Advanced Functional Materials, 16, 1228–1234 (2006)

[124] Kim H. and Hwang T., Effect of Titanium Isopropoxide addition in Low-temperature Cured TiO_2 Photoanode for a Flexible DSSC, Journal of Sol-Gel Science and Technology, 72, 67–73 (2014)

[125] Kubo T., Akitsu K., Uchida S., Segawa H., Otani N., Tomura M., Tamura T. and Matsumura M. Polymer-Sensitized Solar Cells with Novel Soluble Polythiophene Derivatives, Journal of Photopolymer Science and Technology, 23, 283-286 (2010)

[126] IUPAC. McNaught, A.D. and Wilkinson A. (compiled by), Compendium of Chemical Terminology (the "Gold Book"), 2nd ed. Blackwell Scientific Publications, Oxford (1997) (available from: http://goldbook.iupac.org/html/B/B00626.html)

[127] Beer A., Bestimmung der Absorption des rothen Lichts in farbigen Flüssigkeiten (Determination of the absorption of red light in colored liquids), Annalen der Physik und Chemie, 86, 78–88 (1852)

[128] Tams C. and Enjalbert N., Perkin Elmer Application Notes: The Use of UV/Vis/NIR Spectroscopy in the Development of Photovoltaic Cells. PerkinElmer Inc., USA (2009)

[129] Lloyd G.E., Atomic Number and Crystallographic Contrast Images with the SEM: A Review of Backscattered Electron Techniques, Mineralogical Magazine, 51, 3–19 (1987)

[130] Fultz B. and Howe J.M., Transmission Electron Microscopy and Diffractometry of Materials. Springer, Berlin, Heidelberg (2013)

[131] Binnig G., Quate C.F. and Gerber Ch., Atomic Force Microscope, Physical Review Letters, 56, 930–933 (1986)

[132] De Groot P., Principles of interference microscopy for the study of surface topography, Advances in Optics and Photonics, 7, 1–65 (2015)

[133] Conroy M. and Armstrong J., A comparison of surface metrology techniques, Journal of Physics: Conference Series, 13, 458–465 (2005)

[134] Bragg W.H. and Bragg W.L., The reflection of X-rays by crystals Proceedings of the Royal Society of London A, 88, 428–438 (1913)

[135] Albrecht W., Deng T.-S., Goris B., van Huis M.A., Bals S. and van Blaaderen A., Single Particle Deformation and Analysis of Silica-Coated Gold Nanorods before and after Femtosecond Laser Pulse Excitation, Nano Letters, 16, 1818–1825 (2016)

[136] Petrova H., Pérez-Juste J., Pastoriza-Santos I., Hartland G.V., Liz-Marzán L.M. and Mulvaney P., On the temperature stability of gold nanorods: comparison between thermal and ultrafast laser-induced heating, Physical Chemistry Chemical Physics, 8, 814–821 (2006)

[137] Nakade S., Matsuda M., Kambe S., Saito Y., Kitamura T., Sakata T., Wada Y., Mori H. and Yanagida S., Dependence of TiO_2 nanoparticle preparation methods and annealing temperature on the efficiency of dye-sensitized solar cells, Journal of Physical Chemistry B, 106, 10004–10010 (2002)

[138] Epifani M., Helwig A., Arbiol J., Díaz R., Francioso L., Siciliano P., Mueller G. and Morante J.R., TiO_2 thin films from titanium butoxide: Synthesis, Pt addition, structural stability, microelectronic processing and gas-sensing properties, Sensors and Actuators B: Chemical, 130, 599–608 (2008)

ISBN 978-952-12-3705-8